

COMPUTATIONAL AND EXPERIMENTAL STUDY
OF GAN CHEMICAL VAPOR DEPOSITION
REACTOR

By
SUN WONG

A dissertation submitted to the
School of Graduate Studies
Rutgers, The State University of New Jersey
in partial fulfillment of the requirements
for the degree of
Doctor of Philosophy
Graduate Program in Mechanical and Aerospace Engineering

Written under the direction of
Professor Yogesh Jaluria
And approved by

New Brunswick, New Jersey
October, 2017

ABSTRACT OF THE DISSERTATION

Computational and Experimental Study of GaN Chemical Vapor Deposition Reactor

by Sun Wong

Dissertation Director: Professor Yogesh Jaluria

Gallium Nitride is an important semiconductor that many industries use for consumer products such as RF application for celltowers, LED lighting, and HEMTs for power conversion in EV industry. It's the next generation of semiconductor that will be replacing silicon. To produce GaN, many use the technique called Chemical Vapor Deposition or CVD. It's a technique that let gaseous chemicals to react with one another and deposit molecule onto a substrate. As more molecules deposit, it grows into a crystalline structure known as thin film semiconductor. As the demand for high-powered and high-efficiency electronics increases, it's important to look at the quality and characteristics of these films, such as the growth rate, and uniformity. A computational study can be used to model and optimize the CVD reactor to yield favorable operating conditions. With the aid of experimental data, computational CVD study will grant us very important information to help bring down the cost of GaN based semiconductors. A 3D non-reactive model was used initially for flow and temperature study. Then it evolves into a full chemistry model where the growth rate and the uniformity are part of the study. The results are expect to lead to a better understanding of the basic mechanisms for predicting and optimizing the operating conditions. Commercially software was used, with modifications, and the results obtained are discussed in details.

Acknowledgements

First and Foremost, I would like to thank my Ph.D. advisor, Professor Yogesh Jaluria, for supporting me during the past 5 years. He has given me his continuous guidance and encouragement throughout my thesis. Whenever I am stuck at a problem, he would push me to try harder and help me think of ways to overcome the problem. His expertise in the heat transfer field truly remarkable. He is also very patience with me and his other students. It allows us to make mistakes and learn from it. I love how he shared his amazing travel experiences with me and makes me want to see the world even more! He is not only a mentor for my academic career but also my personal life. It has been an honor to be his Ph.D. student.

I would also like to thank Dr. Michael Begarney and Valence Processing Equipment for giving me the opportunity to help them with the research they needed. While I was there, I did not only gain valuable professional experiences, but also gain a good friend. Without Mike's vast knowledge about LEDs, Gallium Nitride and MOCVD reactors, I would be stuck after the first month. Thank you for answering all my questions and there are many many emails! Thank you for showing me that failure isn't really the end but a start to something else. I wish you well in your future endeavors!

I also sincerely thanks my thesis committee, Dr F. Javier Diez-Garias, and Dr. Zhixiong Guo for their supportive suggestions to my Ph.D proposal and thesis. They are both truly great professors at Rutgers. Dr. Diez's research in the Naviator drones is awesome and incredible, but his knowledge in experimental thermal and fluid sciences was even more amazing. Dr. Guo's vast knowledge of heat transfer is outstanding. His advice helped me progress my studies forward. Thank you sincerely for taking time out of your awesome research to help me with my thesis.

Thanks to Dr. Qingze Zou and his assistant for providing me with the AFM images

that I needed for my thesis. I would like to thanks my colleague, Omar Jumaah, for all the help he has giving me with my thesis. He has help me with various of question i had about this thesis and I hope this thesis would give him a good basis for his study.

I would like thank my ex-senior colleague, Dr. Jiandong Meng, for taking the time to explain all the questions I have had throughout my studies. Even after graduating Rutgers, he continue to answer any questions I had email him about. Dr. Han Sun for all the other questions I have in regards to graduate school and classes. THANK YOU!

Thank you to all the engineering staff at Rutgers Mechanical and Aerospace Engineering. Cindy, Carmen, Shefali, and John are the backbone of Rutgers MAE. Without them, I would have even more trouble getting through my graduate studies. Thank you for always answering my questions!

To all my friends I meet at Rutgers. Without you all, life would be so boring. Thanks to everyone that went to have lunch breaks together. Thanks for sharing common hobbies. Thanks for cracking ankle jokes that isnt even funny. Thanks for all the small and long talks. Thanks to everyone that shared C_2H_6O with me. And thank you to all for being there since I started Rutgers and it has been a long time.

The most important acknowledgment is my wife, Katty Siu. I am very grateful to have her part of my life. Without her warm and encouraging words, I probably would have dropped out of graduate school. Thank you for having patience with me throughout my studies. Thank you for being there. No matter if it is up or down, happy or sad, easy or difficult you were always there to support me. I hope we will continue to make more life chapters as this one comes to an end. I <3 U 2 ∞ & ^!

Finally, I am indebted to my parent for their unparalleled support for me.

Thanks to all those I forgot as well!

Table of Contents

Abstract	ii
Acknowledgements	iii
List of Figures	viii
1. Introduction	1
1.1. History	1
1.2. Applications	2
1.3. Current Problems	3
1.4. Motivations	3
1.5. Present Work	4
1.6. Dissertation Outline	4
2. Design of CVD Computational Model	6
2.1. Introduction	6
2.2. Conservation Laws	6
2.3. Chemical Vapor Deposition Process	8
2.4. Chemical Process of Gallium Nitride	10
2.5. Chemistry Model	12
2.6. Computational Method	14
3. Simple Computational Model	17
3.1. Introduction	17
3.2. Simple Computational Model	17
3.3. Validations	21
3.4. Results and Discussion	23

3.5. Conclusion	29
4. Chemical Computational Model without Reaction	30
4.1. Introduction	30
4.2. Simple Chemical Model	30
4.3. Results and Discussion	31
4.4. Conclusion	39
5. Full Chemistry Model	40
5.1. Introduction	40
5.2. Full Chemistry Model	40
5.3. Results and Discussion	43
5.3.1. Effect of Pressure	46
5.3.2. Effect of Inlet Velocity	48
5.3.3. Effect of Susceptor Rotation Speed	50
5.3.4. Effect of V/III Ratio	52
5.4. Conclusion	53
6. Practical Chemical Vapor Deposition Reactors	55
6.1. Introduction	55
6.2. Practical CVD Reactor	55
6.2.1. CVD Environment	56
6.2.2. Vacuum System	57
6.2.3. Heater System	58
6.2.4. Cooling System	58
6.2.5. Rotational Drive System	59
6.2.6. Gas Supply System	60
6.2.7. Measurement System	61
6.2.8. Computer Electronic System	62
6.3. Computational Setup	62

6.4. Computational Results Using Experimental Conditions	63
6.4.1. Sample PR05	64
6.4.2. Sample PR06	66
6.4.3. Sample PR07	68
6.4.4. Sample PR08	70
6.4.5. Sample PR10	71
6.4.6. Sample PR11	74
6.5. Conclusion	74
7. Conclusions	77
7.1. Summary	77
7.2. Future Work	79

List of Figures

2.1. Shaded element indicates it has been deposited by CVD. Adapted from Creighton et al.	11
2.2. Visual representation of chemical reaction of GaN growth	12
2.3. GaN Chemical Pathways for Gas Reactions	13
2.4. GaN Chemical Pathways for Surface Reactions	14
2.5. Chemical Pathway Abbreviation List	15
2.6. GaN Chemical Pathways for Surface Reactions	16
2.7. GaN Chemical Pathways for Gas and Surface Reactions	16
3.1. 3D geometry model for GaN Simulation	18
3.2. Boundary Conditions for 3D Model	19
3.3. Pressure Based Solver Algorithm	20
3.4. Computational and Experimental Temperature Comparison	22
3.5. Computational and Experimental Temperature Comparison	22
3.6. ANSYS Fluent Result of Heated Plate in Ambient Air	23
3.7. ANSYS Fluent Temperature Contour for 0RPM	23
3.8. ANSYS Fluent Velocity Streamlines for 0RPM	24
3.9. ANSYS Fluent Temperature Contour for 300RPM	25
3.10. Flow Visualization - 0RPM	25
3.11. Flow Visualization - 300RPM	26
3.12. ANSYS Fluent Velocity Streamlines for 300RPM	26
3.13. ANSYS Fluent Temperature Gradient for 0.25 m/s	27
3.14. ANSYS Fluent Velocity Streamlines for 0.25 m/s	27
3.15. ANSYS Fluent Temperature Gradient for 2.00 m/s	28
3.16. ANSYS Fluent Velocity Streamlines for 2.00 m/s	28

4.1. ANSYS Fluent Temperature Contour (Air, $V=0.25$ m/s, 60 RPM) . . .	32
4.2. ANSYS Fluent Flow Streamline (Air, $V=0.25$ m/s, 60 RPM)	32
4.3. ANSYS Fluent Temperature Contour (Air, $V=0.25$ m/s, 60 RPM) . . .	33
4.4. ANSYS Fluent Flow Streamline (Air, $V=0.25$ m/s, 60 RPM)	33
4.5. ANSYS Fluent Temperature Contour (N_2 , $V=0.25$ m/s, 0 RPM)	34
4.6. ANSYS Fluent Flow Streamline (N_2 , $V=0.25$ m/s, 0 RPM)	34
4.7. ANSYS Fluent Temperature Contour (N_2 , $V=0.25$ m/s, 60 RPM) . . .	35
4.8. ANSYS Fluent Flow Streamline (N_2 , $V=0.25$ m/s, 60 RPM)	35
4.9. ANSYS Fluent Temperature Contour (H_2 , $V=0.25$ m/s, 0 RPM)	36
4.10. ANSYS Fluent Flow Streamline (H_2 , $V=0.25$ m/s, 0 RPM)	36
4.11. ANSYS Fluent Temperature Contour ($N_2=70\%$ $H_2=30\%$, $V=0.25$ m/s, 0 RPM)	37
4.12. ANSYS Fluent Flow Streamline ($N_2=70\%$ $H_2=30\%$, $V=0.25$ m/s, 0 RPM)	37
4.13. ANSYS Fluent Temperature Contour ($N_2=70\%$ $H_2=30\%$, $V=1$ m/s, 600 RPM)	38
4.14. ANSYS Fluent Flow Streamline ($N_2=70\%$ $H_2=30\%$, $V=1$ m/s, 600 RPM)	38
5.1. Temperature Contour Diagram from Meng <i>et al.</i>	41
5.2. Temperature Contour Diagram from the 11 Eqn Model	41
5.3. Velocity Streamline Diagram from Meng et al.	41
5.4. Velocity Streamline Diagram from the 11 Eqn Model	41
5.5. Deposition Growth Chart from Meng et al.	42
5.6. Deposition Growth Chart from the 11 Eqn Model	42
5.7. Deposition Contour Map from the 11 Eqn Model	42
5.8. Model Comparison. Adapted from Hu et al.	43
5.9. ANSYS Fluent Reactor Conditions - Control	43
5.10. Temperature Contour - Control	44
5.11. Flow Streamlines - Control	45
5.12. Growth Contours - Control	45
5.13. Temperature Contours - Effect of Pressure	46

5.14. Flow Streamlines - Effect of Pressure	47
5.15. Growth Contours - Effect of Pressure	47
5.16. Temperature Contours - Effect of Inlet Velocity	48
5.17. Flow Streamlines - Effect of Inlet Velocity	49
5.18. Growth Contours - Effect of Inlet Velocity	49
5.19. Temperature Contours - Effect of Rotation	50
5.20. Flow Streamlines - Effect of Rotation	51
5.21. Growth Contours - Effect of Rotation	51
5.22. Growth Contours - Effect of Low V/III Ratio	52
5.23. Growth Contours - Effect of High V/III Ratio	53
6.1. Modern Chemical Vapor Deposition Reactors. Source: AIXTRON . . .	55
6.2. Clean Room Class Chart	56
6.3. Vacuum Process Pump	57
6.4. Heater Coils used for CVD Applications	58
6.5. Chill Water System used for CVD Applications	59
6.6. Rotating Susceptor CVD Reactor. Source: AIXTRON	60
6.7. CVD Gas Panel and Bubbler. Source: Google Image Search	61
6.8. In situ Pyrometer and Reflectance Meter.	62
6.9. Computer Electronic System Control Screen.	63
6.10. Model Geometry for the Practical CVD Reactor	63
6.11. Reactor Condition for GaN Growth - Sample PR05	64
6.12. Temperature Contour - Sample PR05	65
6.13. Velocity Streamlines - Sample PR05	65
6.14. GaN Deposition Contour - Sample PR05	65
6.15. SEM Image - Sample PR05	65
6.16. X Ray Diffraction Graph - Sample PR05	66
6.17. Reactor Condition for GaN Growth - Sample PR06	67
6.18. Temperature Contour - Sample PR06	67
6.19. Velocity Streamlines - Sample PR06	67

6.20. GaN Deposition Contour - Sample PR06	67
6.21. Thickness Layer Contour - Sample PR06	67
6.22. SEM Image - Sample PR06	68
6.23. Reactor Condition for GaN Growth - Sample PR07	69
6.24. Temperature Contour - Sample PR07	69
6.25. Velocity Streamlines - Sample PR07	69
6.26. GaN Deposition Contour - Sample PR07	70
6.27. Thickness Layer Contour - Sample PR07	70
6.28. Reactor Condition for GaN Growth - Sample PR08	70
6.29. Temperature Contour - Sample PR08	71
6.30. Velocity Streamlines - Sample PR08	71
6.31. GaN Deposition Contour - Sample PR08	71
6.32. Thickness Layer Contour - Sample PR08	71
6.33. Reactor Condition for GaN Growth - Sample PR10	72
6.34. Temperature Contour - Sample PR10	72
6.35. Velocity Streamlines - Sample PR10	72
6.36. GaN Deposition Contour - Sample PR10	73
6.37. Thickness Layer Contour - Sample PR10	73
6.38. Atomic Force Microscopy Image - Sample PR10	73
6.39. Reactor Condition for GaN Growth - Sample PR11	74
6.40. Temperature Contour - Sample PR11	75
6.41. Velocity Streamlines - Sample PR11	75
6.42. GaN Deposition Contour - Sample PR11	75

Chapter 1

Introduction

1.1 History

Gallium Nitride (GaN) is a group III/V semiconductor compound that allows the production of high powered transmitters, light emitting diodes, transistors, and other Integrated circuit components. [1, 2, 3, 4] GaN was first discovered in 1938 by Juza and Hahn. [5] Small needles and platelets of GaN were synthesized when ammonia was passed over hot Gallium. In 1969, two Ph.D. chemists at Radio Corporation of America named Maruska and Tietjen [6] demonstrated the first single crystal GaN growth using hydride vapor phase epitaxy (HVPE) on a sapphire substrate. This technique uses heated hydrogen chloride to react to group III metals to produce a gaseous phase metal chloride then further react with ammonia to produce the group III nitride. In 1983 Yoshida [7] et al. grew GaN film using a technique called reactive molecular beam epitaxy or MBE. It is a deposition technique where each atom is deposit one at a time in an orderly manner. Due to the heavy contamination and low efficiency in the GaN film using the HVPE process, many researchers abandon this projects. It was 1984 when a new breakthrough in GaN fabrication process began. Kawabata et al. [8] at Matsushita was the first to grow blue LED GaN using Metal Organic Chemical Vapor Deposition (MOCVD). In 1986, Amano et al. [9] improve the process using the buffer layer concept that improved the structural quality. In 1988, Amanos group further improved the luminescence of the film by using Zinc doped GaN grown by MOCVD. However, the GaN film cannot achieve a true blue LED because the band gap energy was 364 nm. To move the band gap into the visible spectrum, other materials was added to create an alloy film. This was what Nakamura [10] did in 1994 to yield a true blue LED. High brightness, high intensity InGaN/AlGaN blue light emitting diodes

were introduced in 1994. The power output were 1500 W and wavelength peaked at 450 nm. It was the brightest LED at the time. By 2012, high powered GaN based LEDs are grown commercially by company like OSRAM. Even till today countless hours of research and development are put into producing low cost, high efficient UV and bright white LEDs.

1.2 Applications

GaN films are used widely as a semiconductor materials. The attractive physical properties such as strong chemical and thermal stability, wide bandgap, and high electron mobility makes it a preferred material in wireless RF equipment, MOSFET/HEMT, power generation, sensors, and magneto-optoelectronic equipment.[11, 12, 13, 14, 15] However, most notable use of the GaN is still as an optoelectronic light source. While blue LED has been in development for decades, white LEDs are the current highlights. Using a GaN on Si, scientist was able to develop a low cost white LED into the lightning market. With higher efficiency, brighter and longer life than incandescent bulb, many consumers are switching to LED for their choice of lightning. Another use of GaN based electronics are High Electron Mobility Transistors (HEMTs) and field effect transistors (FETs) in RF communications. Many of the current RF communication equipment uses Gallium Arsenide (GaAs) or Silicon (Si) as the semiconductor material. As the demand for higher power equipment increase, many of the industries started to use GaN as the replacement, therefore demands of GaN based semiconductors increases. The greater transmitting power and higher efficiencies supplied by the GaN based materials means fewer of the same equipment is needed for the same job such as satellites and cell towers. Some recent application such as GaN nanotubes are also being produced by CVD. Using GaN nanotube in optoelectronic application, such as sensors, will greatly increases the sensitivity and resolutions of the device.

1.3 Current Problems

The use of GaN based semiconductor is still a very young technology compared to other semiconductor materials such as silicon.[16, 17, 18] Even with many decades of improvements, there are still challenges that prevent GaN from going mass production at a low cost. As described in the previous section, lattice mismatch is one of the many problems. Growth rates, and uniformity are some of other few major problems industry are facing. There is a trade-off between quality and the throughput. Higher the quality, the lower the system produces and higher the price. To lower the cost, high throughput systems are more desired, however film quality is sacrificed. Many industries incorporate geometry design to help increase film quality in a high throughput systems such as a rotating susceptor. However, chemical vapor deposition and other vapor growth technique still requires the chemical reaction itself. To achieve a chemical reaction for crystalline growth, internal reactor condition must be maintaining at favorable environments. Chemical concentrations, flow rates, pressure and temperature are all involved in creating that condition. While geometry cannot be easily change, these other conditions parameter can be change easily to improve the quality of the crystalline film structure. Industry has named these fine-tuned conditions as recipe, and they developed an ideal recipe for each certain geometry by months and years of running various conditions. Developing these ideal recipe has a very big cost, and it needs to be improved. By understanding chemical kinetics, computational method can be used to model and simulate GaN growth.

1.4 Motivations

The current technology behind Gallium Nitride and Chemical Vapor Deposition can certainly be improved. Uniformity and growth rates are still issues that need to be improved on. As industries step up to produce larger wafers, 4 inches and larger, the uniformity and quality of the wafer decreases. Even for the smaller wafer designs, industries have been using excessive raw material to yield satisfactory level of output. The typical throughput of GaN wafer is still very low which yield a high cost of production.

In the current market, one 100 mm diameter silicon wafer cost about \$25 - \$50. One 100 mm diameter silicon on sapphire wafer cost about \$600 to \$700. However, the cost for one 100mm diameter GaN on sapphire wafer cost about \$850 to \$950 and it would cost even more for a GaN on GaN substrate. It is important to optimize the use of raw material to keep the cost down for consumers. The motivation for this thesis is to start investigating the fundamental theory behind Chemical Vapor Deposition and Gallium Nitride and develop a computation model to simulate the CVD process in the reactor. By understanding the characteristic of the flow and heat transfer inside the reactor chamber, we can accurately model the chamber by computational method. Then using the computational result data as an input for the operating condition of experimental CVD system. Data from the experimental system can also be used to input as initial condition for the computer model simulation.

1.5 Present Work

There are many studies about chemical vapor depositions especially with specific materials and computational models, but very limited investigation in experimental study of the rotational reactors. The present work involves an experimental study in a rotational reactor at atmospheric pressure. Air will be used as the material to conduct the study of the temperature profiles and flow characteristics inside the reactor. Altering the flow inside a highly buoyancy reactor by inducing a rotational effect will yield a more favorable film growth conditions. Understanding these parameters will aid in developing model that can predict operating conditions for different type of crystal growth more efficiently. Computational model that was validated with experimental result shows a more similar results than just computational studies alone.

1.6 Dissertation Outline

- Chapter 1: (Current chapter) This chapter gives a background of Gallium Nitride and Chemical Vapor Deposition. It also has a simplified explanation of the

chemical pathway of Gallium Nitride. More in-depth analysis of the chemical reaction pathway will discuss in later chapter. Some of the current challenges that industry are facing are also listed in this chapter.

- Chapter 2: This chapter focus on the development of the chemical vapor deposition model. Conservation laws are described and well as the chemical process of Gallium Nitride.
- Chapter 3: The chapter will focus on the simple geometry computational model. Explanation of the computational model and validation study also be discussed to give the basis and accuracy of this model. Computational data will also show here. It will shows effect of changes when certain conditions are modified.
- Chapter 4: The next step where the simple model with species transport added would be shown here. Species gases are introduced in this chapter. A more in depth study of how chemical species affect the flow and heat transfer inside the reactor chamber. Interpretation of the data are also presented in this chapter
- Chapter 5: Third step of the simple model will include chemical reactions. Computation will be based on the full chemistry model. In addition to flow and heat transfer data, deposition data will also presented. It will also show the effect to the flow, heat transfer and deposition as growth conditions are change.
- Chapter 6: Final step of the study will be the use of a practical CVD reactor. A detail breakdown of how a practical CVD reactor is set up. A new geometry is adapted from the practical CVD reactor and used in the computational study. Experimental conditions was used as conditions for the computational model and the results are compared with experimental samples.
- Chapter 7: This chapter finalize and summarize my study for this thesis. I will also contain future work that need to be done to further improve the model.

Chapter 2

Design of CVD Computational Model

2.1 Introduction

Designing and modeling the chemical vapor deposition reactor for gallium nitride requires understanding of governing equations. We understand precursor gases flow into the chamber, undergo various chemical reactions, and then exit the chamber while the chamber is maintained at certain temperature and pressure. We can view this problem as a complex fluid dynamic problem. Using Conservation of Mass, Momentum, Energy and Species, we can represent most of the variables that are involved inside the reactor chamber. The chemical reaction would be an addition module incorporate to the fluid problem. This chemistry model would control the rate processes, and the transport properties of the various chemical species. A detail breakdown explanation would be discuss in the following sections.

2.2 Conservation Laws

Conservation laws are the basic principle of physics that governs all mechanics. It states that in an isolated control physical volume, the measurable quantities are neither created nor destroyed however, it can be converted into another form or transferred from one to another. In a chemical vapor deposition reactor, we can consider the entire inside of the reactor chamber to be the isolated physical volume. Conservation laws can now be used to interpret the measurable quantities that are presented in the reactor chamber. There are 4 total conservation laws that are being used in this study. These are the conservation of mass, momentum, energy and species.

Solving the full version of conservation laws will require a lot of time even for a

computational model. It is good practice to reduce or simplify the equations by the use of logical assumptions that can be apply to the CVD reactor. According to Jones et al [2], in a typical chemical vapor deposition process, the convective transport, diffusive transport, and chemical reaction are combinations of low velocities and often reduce pressure that lead to low Reynolds numbers. Gas flow within the CVD reactors is nearly always laminar, therefore in the design and analysis of CVD processes, it is not necessary to consider turbulence. Viscous dissipation can be neglect because of the low velocities of the flows. Ideal gas and Newtonian fluid assumptions are also considered. A simplified version of the conservation law is shown below. Conservation of mass:

$$\frac{\partial \rho}{\partial t} + \nabla \cdot (\rho \mathbf{V}) = 0 \quad (2.1)$$

Conservation of momentum:

$$\frac{\partial \rho \mathbf{V}}{\partial t} + \nabla \cdot (\rho \mathbf{V} \mathbf{V}) = -\nabla p + \nabla \cdot \tau + \rho \mathbf{g} \quad (2.2)$$

Conservation of energy:

$$\frac{\partial \rho h}{\partial t} + \nabla \cdot (\rho h \mathbf{V}) = \nabla \cdot (\lambda \nabla T) + \nabla \cdot (\tau \cdot \mathbf{V}) + S_h \quad (2.3)$$

Conservation of species:

$$\frac{\partial \rho \Phi_i}{\partial t} + \nabla \cdot (\rho \Phi_i \mathbf{V}) = \nabla \cdot (\rho D_i \nabla \Phi_i) + M_i \dot{w}_i + S_{\Phi} \quad (2.4)$$

Equation of state for gas mixture:

$$\rho = \frac{p}{RT} \sum \frac{\Phi_i}{M_i} \quad (2.5)$$

Constraint on mass fractions:

$$\sum_{i=1}^{N_s} \Phi_i = 1 \quad (2.6)$$

where ρ , \mathbf{V} , p , h , T , g , R , and Φ_i are density of the gas mixture, dynamic pressure,

enthalpy of gas mixture, temperature, gravitational acceleration, universal gas constant, and mass fraction of each of the N_s species respectively; λ is the thermal conductivity of the gas mixture; D_i is mass diffusivity of the species i ; M_i and \dot{w}_i are molecular weight of the species i and its molar production rate per unit volume due to gas-phase reactions, respectively. The shear stress, and source terms in the energy and species equations are expressed as:

$$\tau = \mu(\nabla \mathbf{V} + \nabla \mathbf{V}^T) - \frac{2}{3}\mu(\nabla \cdot \mathbf{V})\mathbf{I} \quad (2.7)$$

$$S_h = \frac{\partial p}{\partial t} + \nabla \cdot q_R + \nabla \cdot (\sum_{i=1}^{N_s} h_i j_i) - \sum_{i=1}^{N_s} h_i M_i \dot{w}_i \quad (2.8)$$

The species diffusive flux, j_i is defined as

$$j_i = \rho D_i \nabla \Phi_i + \frac{\rho \Phi_i}{M} D_i \nabla M - M \Sigma_j D_j \nabla \Phi_j - \nabla M \Sigma_j D_j \Phi_j + \frac{\rho D_i^T \nabla T}{T} - \rho \Phi_i \Sigma_j \frac{D_j^T \nabla T}{T} \quad (2.9)$$

$$S_\Phi = \nabla \cdot \left(\frac{\rho \Phi_i}{M} D_i \nabla M + \frac{\rho D_i^T \nabla T}{T} - \rho \Phi_i \Sigma_j \frac{D_j^T \nabla T}{T} - M \Sigma_j D_j \nabla \Phi_j - \nabla M \Sigma_j D_j \Phi_j \right) \quad (2.10)$$

where μ , q_R , D_i^T and h_i are the mixture dynamic viscosity, radiation heat flux, the soret diffusion coefficient of species i and the enthalpy of species i respectively; \mathbf{I} is a unit tensor; M is the molecular weight of the gas mixture.

2.3 Chemical Vapor Deposition Process

Chemical Vapor Deposition is a heat activated process that involves the use of gases and vapors. There are combination of gases and vapors present inside the chamber, so it is also important to know the properties and the flow characteristics of the materials. There are 4 type of gases used in a CVD reactor: Precursor, Carrier, Reactive, and Dopant. Precursor gases are the raw materials such as TrimethylGallium (TMGa) and

the outcome would be GaN. Raw material that are not in gaseous form will undergo a phase change before entering the chamber. Liquid materials such as TMGa will be placed in a temperature controlled apparatus called bubbler to convert the liquid form into a vapor form. Both gaseous and vapor state material is transported into the chamber by the carrier gas. The sole purpose of the carrier gas is to transport other gases and vapor into and out of the chamber. Typical carrier gas used are Nitrogen (N_2), or Argon (Ar) due to their inert characteristics. Reactive gas reacts to the precursor gas to produce the desired material. The reactive gas use for GaN is Ammonia (NH_3). As the TMGa and NH_3 undergo chemical reactions, the decomposition is deposited on to the surface substrate. This new material on the surface is the crystalline film structure, and as more reaction occurs the faster the growth of this film. Last type of gas is called Dopant. As more and more complex materials are used, the more byproduct it will produce in the system and some of these byproduct are radicals molecule that will reacts to other material causing impurities in the film growth. Impurities in the crystalline structure reduces the strength that causes cracks or discontinuities in the material. Dopant gases are used to neutralize these radicals molecule to promote growth rates and uniformity of desired materials.

Chemical reaction only occurs when the system has enough energy, and this energy is fuel by the heat transfer that occurs between the heaters and the chamber. Some of these heater source can be microwave heating, induction coil heating or resistive heating. It is important to control the heating of the chamber, since thermal energy initiate the chemical reactions. Not enough thermal energy, there would be low growth rates, and increase in raw material waste and byproducts. This region is called Kinetics-Limited Regime. Too much thermal energy will cause the process to burn up or desorption occurs. This region is called Thermodynamics-Limited Regime. The area where growth rate is optimal is called Diffusion Controlled Regime.

As the chamber heats up to the desired temperatures, the precursor gas and the reactive gas molecules begin to break apart from the surrounding thermal energy or adsorption phase. After molecules are in their radical forms, they react with other radicals and recombines to form the new materials. This is the reaction phase and

it occurs usually near the substrate surface. Concurrently, excessive byproducts and energies are released from the new materials back into the free stream. This is the desorption phase. The new material is deposited onto the substrate and it begins to grow in thickness as more and more chemical reaction occurs. The byproduct exits the chamber as more precursor and reactive gas enters the chamber. The temperature, pressure and flow rates of these chemical during the process plays an important role in controlling uniformity and growth rates. Almost all CVD reactors follow these steps.

The precursor gases falls under one of these categories. First type is called Halides, this chemical group contains one part halogen atom such as Sodium Chloride (NaCl) or Titanium Tetrachloride (TiCl_4). Second type are called Hydrides. This group of metalloids contains hydrogen in the compound such as Silane (SiH_4) or Ammonia (NH_3). Third type are called Metal Organics groups. This type split into more known subcategories called Alkyls, Alkoxides, and Carbonyls. Alkyls are alkane missing one hydrogen atom such as methyl (CH_3). Alkoxides are metal organic group bounded to a negatively charged oxygen atom. It is usually produced from an alcohol group. Carbonyls are molecules that contains a carbon atom double bonded to an oxygen atom with other transitional metal. Currently there are many chemicals that can be deposit by the CVD process and each precursor material is chosen based on material property, decomposition temperatures, vapor pressure of the precursor gas, safety and the cost of the material. Fig. 2.1 shows all the materials that has been deposited by CVD process. [19]

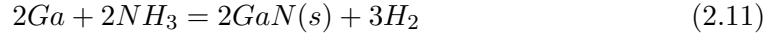
2.4 Chemical Process of Gallium Nitride

Gallium Nitride is a wide band gap material with excellent characteristic for many applications as stated in previous sections. However, many extended applications have been hindered by the production of high quality crystalline films due to crystalline lattice mismatches. A closer look in the chemical pathway process of GaN would help understand the basic of GaN production. In a typical pathway, GaN is produced in the following pathway.

PERIODIC TABLE																	
IA	IIA	IIIA	IVA	VA	VIA	VIIA	VIII			IB	IIIB	IIIB	IV	VA	VIB	VIB	O
1 H 1.008																	2 He 4.003
3 Li 6.941	4 Be 9.012											5 B 10.81	6 C 12.01	7 N 14.01	8 O 16.00	9 F 19.00	10 Ne 20.179
11 Na 22.990	12 Mg 24.305											13 Al 26.98	14 Si 28.06	15 P 30.97	16 S 32.07	17 Cl 35.45	18 Ar 39.948
19 K 39.098	20 Ca 40.08	21 Sc 44.956	22 Ti 47.90	23 V 50.942	24 Cr 51.996	25 Mn 54.938	26 Fe 55.847	27 Co 58.933	28 Ni 58.70	29 Cu 63.546	30 Zn 65.39	31 Ga 69.72	32 Ge 72.61	33 As 74.92	34 Se 78.96	35 Br 79.90	36 Kr 83.80
37 Rb 85.468	38 Sr 87.62	39 Y 88.906	40 Zr 91.22	41 Nb 92.906	42 Mo 95.94	43 Tc (99)	44 Ru 101.07	45 Rh 102.905	46 Pd 106.4	47 Ag 107.868	48 Cd 112.4	49 In 114.8	50 Sn 118.7	51 Sb 121.8	52 Te 127.6	53 I 126.9	54 Xe 131.30
55 Cs 132.905	56 Ba 137.33	57 La 138.9	72 Hf 178.49	73 Ta 180.948	74 W 183.85	75 Re 186.2	76 Os 190.2	77 Ir 192.22	78 Pt 195.09	79 Au 196.966	80 Hg 200.59	81 Tl 204.37	82 Pb 207.2	83 Bi 209.0	84 Po (210)	85 At (210)	86 Rn (222)
87 Fr (223)	88 Ra (226)	89 Ac 227.0															

LANTHANIDES	57 La 138.5	58 Ce 140.115	59 Pr 140.1	60 Nd 144.2	61 Pm (145)	62 Sm 150.4	63 Eu 152.0	64 Gd 157.2	65 Tb 158.9	66 Dy 162.5	67 Ho 164.9	68 Er 167.3	69 Tm 168.9	70 Yb 173.0	71 Lu 174.96
ACTINIDES	89 Ac 227.0	90 Th 232.0	91 Pa 231.0	92 U 238.0	93 Np 237.0	94 Pu (244)	95 Am (243)	96 Cm (247)	97 Bk (247)	98 Cf (251)	99 Es (252)	100 Fm (257)	101 Md (256)	102 No (259)	103 Lr (257)

Figure 2.1: Shaded element indicates it has been deposited by CVD. Adapted from Creighton et al.



However, Gallium is achieved by decomposition of TrimethylGallium or TMGa/ $Ga(CH_3)_3$ first. The decomposition of TMGa is very complex and creates many radical during each step of decomposition. The current known GaN pathway is shown below.

As schematic of the process is shown below.

The process consist of 2 type of reactions: Gas reaction and surface reaction. The gas reaction decompose the TMGa and NH_3 into Ga, and N radicals needed for the surface reaction. Other byproducts are removed from reactor as new precursor are introduced into the reactor chamber. The end product of the surface reaction is the GaN crystalline structure. If the byproduct or radical are not removed from the reaction chamber, it will cause impurities in the crystalline growth. The impurities changes growth rates, thickness of growth layers and structure or lattice. Also substrate interface is another effect of mismatch lattice. If the substrate is of different materials, such as sapphire or Si. There would be discontinuity on the interface because of the different crystalline lattice and material properties of the substrate. Many researcher and commercial producer has alleviate the problems by the use of buffer layers to reduce

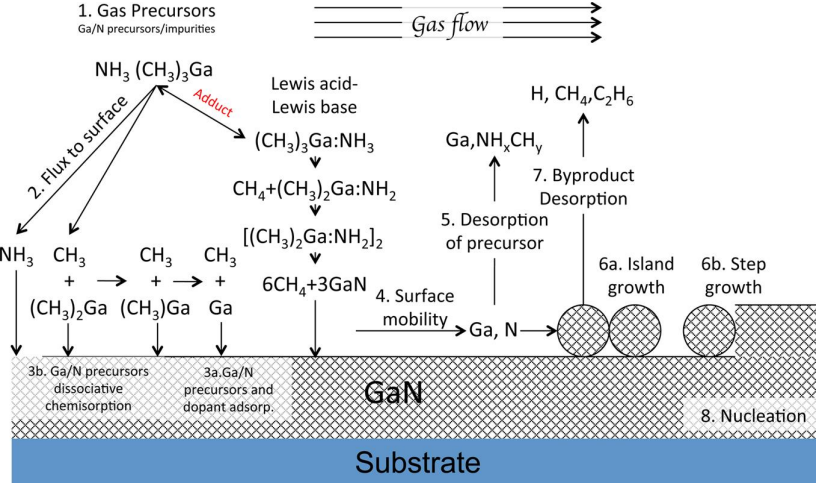


Figure 2.2: Visual representation of chemical reaction of GaN growth

mismatches, and improve quality. Various methods was used to achieved the output of quality crystalline GaN film and one of these methods was trial and error of various conditions when growing GaN in the reactor. However, due to high cost and waste, a more economical way approach is needed to further improve the chemical process of GaN.

2.5 Chemistry Model

The main pathway of the synthesized GaN is shown in equation 2.11. However, a complete transport of the chemical pathway is needed for the chemistry model. All homogeneous and heterogeneous chemical reaction need to be considered and many groups has started to look into the full model. As mentioned before, the process consists of 2 type of reactions: gas reaction and surface reactions. Sengupta et al [20] and Hirako et al [21], presented a sixty-nine (69) chemical pathway equations that would model gallium nitride growth. The 69 equations are broken down to 17 gas reactions and 52 surface reactions. Fig. 2.3, Fig. 2.4 and Fig. 2.5 shows the reaction pathways for this model.

Hu et al [22] used a Rate of Production or ROP analysis to determine the contribution of each of the chemical pathways to the net production or destruction rate of

No.	Gas phase reactions			A	n	E/R
G1	TMGa	\leftrightarrow	DMGa + CH ₃	1.6×10^{17}	0	30057
G2	DMGa	\leftrightarrow	MMGa + CH ₃	2.5×10^{15}	0	17883
G3	MMGa	\leftrightarrow	Ga + CH ₃	4.3×10^{13}	0	24519
G4	TMGa + NH ₃	\rightarrow	TMGa·NH ₃	2.28×10^{31}	-8.31	1568
G5	TMGa + NH ₃	\rightarrow	(CH ₃) ₂ GaNH ₂ + CH ₄	17	2.0	10050
G6	DMGa + NH ₃	\rightarrow	DMGa·NH ₃	4.08×10^{28}	-7.03	1628
G7	DMGa + NH ₃	\rightarrow	CH ₃ GaNH ₂ + CH ₄	530	1.56	10440
G8	MMGa + NH ₃	\rightarrow	MMGa·NH ₃	7.95×10^{21}	-5.21	1054
G9	MMGa + NH ₃	\rightarrow	GaNH ₂ + CH ₄	8.1×10^2	1.3	8919
G10	NH ₃ + CH ₃	\leftrightarrow	NH ₂ + CH ₄	3.31	2.51	4962
G11	CH ₃ + H ₂	\leftrightarrow	CH ₄ + H	1.2×10^9	0	6300
G12	TMGa + H	\leftrightarrow	DMGa + CH ₄	5.0×10^{10}	0	5051
G13	DMGa + H	\leftrightarrow	MMGa + CH ₄	5.0×10^{10}	0	5051
G14	TMGa·NH ₃	\leftrightarrow	MMGa + 2CH ₃ + NH ₃	1.33×10^{44}	-8.24	39150
G15	CH ₃ + H + M	\leftrightarrow	CH ₄ + M	2.4×10^{19}	-1	0
G16	2CH ₃	\leftrightarrow	C ₂ H ₆	2.0×10^{10}	0	0
G17	2H + M	\leftrightarrow	H ₂ + M	1.0×10^{13}	0	0

Figure 2.3: GaN Chemical Pathways for Gas Reactions

a species. It enables identification of the most dominant reactions and combination of intermediate reactions. The analysis was performed on the 52 surface reactions. After the analysis, the numbers of pathways for surface reactions was reduced to 17. This give a total of 34 chemical pathways, 17 gas reactions from the original model and 17 surface reactions from the current improvement.

Hu et al further improved the model by investigating the temperature range of TMGa. TMGa tends to form an adduct with NH₃ when it is in the low temperature zone from 600K to 800K. The temperature for growing GaN for blue LED are well above 1000K. Therefore, many of the adduct chemical pathways can be reduced. At temperature greater than 1000K, all TMGa is consumed and immediately forming MMGa, and all adduct assumption are negligible. This reduces the total gas Reactions to 1 main pathway and further reduce the 17 surface reaction pathways to 10 reaction pathways. Total chemical pathways is now reduced to 11. This reduction of chemical pathways will greatly reduce computational time. Figure 2.7 shows the 11 major chemical pathways for a Gallium Nitride growth. Both the 69 equations model and the 11 equations model will be used in this thesis.

No.	Surface reaction		A	n	E/R	
S1	MMGa + S _N	→	MMGa(s)	1.160×10 ⁵	2.98	0
S2	MMGa(s)	→	MMGa + S _N	1.115×10 ¹⁴	0.55	5.4189×10 ⁴
S3	NH ₃ + MMGa(s)	→	COMPM1(s)	3.354×10 ⁷	3.33	0
S4	COMPM1(s)	→	NH ₃ + MMGa(s)	5.700×10 ¹³	-0.16	4.1000×10 ³
S5	MMGa + COMPM1(s)	→	CH ₄ + COMPM2(s)	1.230×10 ¹⁰	3.22	1.1800×10 ⁴
S6	NH ₃ + COMPM2(s)	→	COMPM3(s)	3.354×10 ⁷	3.33	0
S7	COMPM3(s)	→	NH ₃ + COMPM2(s)	5.700×10 ¹³	-0.161	4.1000×10 ³
S8	MMGa + COMPM3(s)	→	CH ₄ + COMPM4(s)	1.230×10 ¹⁰	3.22	1.1800×10 ⁴
S9	NH ₃ + COMPM4(s)	→	COMPM5(s)	3.354×10 ⁷	3.33	0
S10	COMPM5(s)	→	NH ₃ + COMPM4(s)	5.700×10 ¹³	-0.161	4.1000×10 ³
S11	COMPM5(s)	→	CH ₄ + RINGM1S(s)	1.230×10 ¹⁰	3.22	1.1800×10 ⁴
S12	S _G + RINGM1(s)	→	RINGM2(s)	3.354×10 ⁷	3.33	0
S13	RINGM2(s)	→	3H ₂ + 3GaN + S _G + S _N	3.680×10 ⁹	2.05	3.0000×10 ⁴
S14	CH ₃ + Ga(s)	→	MMGa(s)	1.760×10 ⁹	1.39	0
S15	MMGa(s)	→	CH ₃ + Ga(s)	4.540×10 ¹³	0.0346	4.0000×10 ⁴
S16	NH ₂ + S _G	→	NH ₂ (s)	3.168×10 ⁸	1.83	0
S17	GaNH ₂ + S _N	→	GaNH ₂ (s)	2.273×10 ⁶	2.247	0
S18	GaNH ₂ (s)	→	GaNH ₂ + S _N	4.826×10 ¹³	0.614	4.2215×10 ⁴
S19	COMPM1(s)	→	CH ₄ + GaNH ₂ (s)	1.490×10 ¹¹	0.609	1.3060×10 ⁴
S20	MMGa + GaNH ₂ (s)	→	COMPMM1(s)	1.160×10 ⁵	2.98	0
S21	NH ₃ + COMPMM1(s)	→	COMPMM2(s)	3.354×10 ⁷	3.33	0
S22	COMPMM2(s)	→	CH ₄ + COMPMM3(s)	1.490×10 ¹¹	0.609	1.3060×10 ⁴
S23	MMGa + COMPMM3(s)	→	COMPMM4(s)	1.160×10 ⁵	2.98	0
S24	NH ₃ + COMPMM4(s)	→	COMPMM5(s)	3.354×10 ⁷	3.33	0
S25	COMPMM5(s)	→	CH ₄ + RINGM1(s)	1.490×10 ¹¹	0.609	1.3060×10 ⁴
S26	NH ₂ (s)	→	NH ₂ + S _G	1.450×10 ¹⁴	0.09	3.0089×10 ⁴
S27	COMPMM1(s)	→	MMGa + GaNH ₂ (s)	1.000×10 ¹⁴	0.55	2.1550×10 ⁴
S28	COMPMM2(s)	→	NH ₃ + COMPMM1(s)	5.700×10 ¹³	-0.1	4.1000×10 ³
S29	COMPMM4(s)	→	MMGa + COMPMM3(s)	1.000×10 ¹⁴	0.55	2.1550×10 ⁴
S30	COMPMM5(s)	→	NH ₃ + COMPMM4(s)	5.700×10 ¹³	-0.1	4.1000×10 ³
S31	Ga + S _N	→	Ga(s)	1.000×10 ¹¹	1.50	0
S32	Ga(s) + NH ₂ (s)	→	GaNH ₂ (s) + S _G	1.000×10 ²⁵	0.0	0
S33	Ga(s)	→	Ga + S _N	1.000×10 ¹³	0.0	2.2732×10 ⁴
S34	6CH ₃ + RINGM2(s)	→	COM1(s)	7.550×10 ⁷	2.31	0
S35	COM1(s)	→	6CH ₃ + RINGM2(s)	1.000×10 ¹³	0.71	2.2902×10 ⁴
S36	COM1(s)	→	6CH ₄ + 3GaN + S _G + S _N	4.000×10 ¹²	0.0	2.5000×10 ⁴
S37	TMGa + S _N	→	TMGa(s)	1.160×10 ⁵	2.98	0
S38	NH ₃ + TMGa(s)	→	TCOM1(s)	3.354×10 ⁷	3.33	0
S39	TCOM1(s)	→	CH ₄ + TCOM2(s)	1.490×10 ¹¹	0.609	1.6500×10 ⁴
S40	S _G + TCOM2(s)	→	TCOM3(s)	3.354×10 ⁷	3.33	0
S41	TCOM3(s)	→	2CH ₄ + GaN + S _G + S _N	1.490×10 ¹¹	0.609	2.5000×10 ⁴
S42	TMGa(s)	→	TMGa + S _N	1.115×10 ¹⁴	0.55	2.5000×10 ⁴
S43	TCOM1(s)	→	NH ₃ + TMGa(s)	5.700×10 ¹³	-0.161	6.0000×10 ⁴
S44	TMGa NH ₃ + S _N	→	TCOM1(s)	1.160×10 ⁵	2.98	0
S45	TCOM1(s)	→	TMGa NH ₃ + S _N	1.115×10 ¹⁴	0.55	2.5000×10 ⁴
S46	TCOM1(s)	→	2CH ₃ + MMGa + NH ₃ + S _N	1.115×10 ¹⁴	0.55	5.4189×10 ⁴
S47	MMGa NH ₃ + S _N	→	COMPM1(s)	1.160×10 ⁵	2.98	0
S48	COMPM1(s)	→	MMGa NH ₃ + S _N	1.115×10 ¹⁴	0.55	5.4189×10 ⁴
S49	MMGa NH ₃ + COMPM1(s)	→	CH ₄ + COMPM3(s)	1.230×10 ¹⁰	3.22	1.18×10 ⁴
S50	MMGa NH ₃ + COMPM3(s)	→	CH ₄ + COMPM5(s)	1.230×10 ¹⁰	3.22	1.18×10 ⁴
S51	MMGa NH ₃ + GaNH ₂ (s)	→	COMPMM2(s)	1.160×10 ⁵	2.98	0
S52	MMGa NH ₃ + COMPMM3(s)	→	COMPMM5(s)	1.160×10 ⁵	2.98	0

Figure 2.4: GaN Chemical Pathways for Surface Reactions

2.6 Computational Method

Computational model can be very complicated, especially when modeling a complex system with gases, liquid and solids. In a normal model, the entire geometry is imported into the computational solver and every part of the geometry must be defined for the computational mode to work. This can cause errors if some part are not defined correctly. To simplify the entire modeling, only the control volume will be used for modeling. Currently the simple model that was set up is a cone shape model. Which will describe in detail in the later chapter. There is a rotating susceptor on the bottom. This type of reactor is called a vertical impinging because flows comes in from the top

Name	Chemical formula
COMPM1	$\text{NH}_3 \text{ MMGa(s)}$
COMPM2	$\text{Ga NH}_2 \text{ MMGa(s)}$
COMPM3	$\text{NH}_3 \text{ Ga NH}_2 \text{ MMGa(s)}$
COMPM4	$\text{Ga NH}_2 \text{ Ga NH}_2 \text{ MMGa(s)}$
COMPM5	$\text{NH}_3 \text{ Ga NH}_2 \text{ Ga NH}_2 \text{ MMGa(s)}$
COMPMM1	$\text{MMGa GaNH}_2\text{(s)}$
COMPMM2	$\text{NH}_3 \text{ MMGa} \cdot \text{NH}_2 \text{ Ga(s)}$
COMPMM3	$\text{NH}_2 \text{ Ga} \cdot \text{NH}_2 \text{ Ga(s)}$
COMPMM4	$\text{MMGa NH}_2 \text{ Ga NH}_2 \text{ Ga(s)}$
COMPMM5	$\text{NH}_3 \text{ MMGa NH}_2 \text{ Ga NH}_2 \text{ Ga(s)}$
TCOM1	$\text{NH}_3 \text{ TMGa(s)}$
TCOM2	$\text{NH}_2 \text{ DMGa(s)}$
TCOM3	$\text{(s)NH}_2 \text{ DMGa(s)}$
RINGM1	$\text{NH}_2 \text{ Ga NH}_2 \text{ Ga NH}_2 \text{ Ga(s)}$
RINGM2	$\text{(s)NH}_2 \text{ Ga NH}_2 \text{ Ga NH}_2 \text{ Ga(s)}$
COM1	$\text{RINGM2 } 6\text{CH}_3$

Figure 2.5: Chemical Pathway Abbreviation List

and impinges on the rotating susceptor. The space between the cone and the susceptor will be the control volume used for modeling. It is assume to be a pseudo fluid medium in the model that holds the shape by defined boundary conditions. This reduces the complexity to only few boundary conditions.

The model is imported into a software called ANSYS Fluent. Fluent is a computational fluid dynamic software that allows multiphysics module to be added to the computation. The model will include fluid dynamic, heat transfer, species transport and chemical reactions. TO understand the model in detail, multiple steps will be taken before incorporating all the module together. First step will solve the fluid dynamic and heat transfer part only, then species transport will be added to step two, and finally step three will include chemical reactions. The computational model will require to the use of hardwares. For the entirely of the study, the computational model was run on a personal computer with 8 core processor, 32Gb of RAM, and a 2Gb quad core graphic card for the supplementary processing power.

	$k=AT^n e^{-Ea/RT}$				A	n	Ea
<i>G1</i>	TMG	=	DMG	+ CH ₃	1.00E+47	-9.18	76996
<i>G2</i>	DMG	=	MMG	+ CH ₃	7.67E+43	-9.8	34017
<i>G3</i>	MMG	=	Ga	+ CH ₃	1.68E+30	-5.07	84030
<i>G4</i>	TMG	+	NH ₃	→ TMG:NH ₃	2.28E+34	-8.31	3115
<i>G5</i>	TMG	+	NH ₃	→ DMG:NH ₂ + CH ₄	1.70E+04	2	19969
<i>G6</i>	DMG	+	NH ₃	→ DMG:NH ₃	4.08E+31	-7.03	3234
<i>G7</i>	DMG	+	NH ₃	→ MMG:NH ₂ + CH ₄	5.30E+05	1.56	20744
<i>G8</i>	MMG	+	NH ₃	→ MMG:NH ₃	7.95E+24	-5.21	2094
<i>G9</i>	MMG	+	NH ₃	→ GaNH ₂ + CH ₄	8.10E+05	1.3	17722
<i>G10</i>	NH ₃	+	CH ₃	→ NH ₂ + CH ₄	3.31E+03	2.51	9859
<i>G11</i>	CH ₃	+	H ₂	→ CH ₄ + H	1.20E+12	0	12518
<i>G12</i>	TMG	+	H	→ DMG + CH ₄	5.00E+13	0	10036
<i>G13</i>	DMG	+	H	→ MMG + CH ₄	5.00E+13	0	10036
<i>G14</i>	TMGNH ₃	→	MMG	+ 2CH ₃ + NH ₃	1.33E+44	-8.24	77791
<i>G15</i>	CH ₃	+	H	+ M → CH ₄ + NH ₃	2.40E+22	-1	0
<i>G16</i>	2CH ₃	=	C ₂ H ₆		2.00E+13	0	0
<i>G17</i>	2H	+	M	= H ₂ + M	2.00E+16	0	0

Figure 2.6: GaN Chemical Pathways for Surface Reactions

	Gas Reaction, $k=AT^n e^{-Ea/RT}$				A	n	Ea
<i>1</i>	TMG	→	MMG	+ C ₂ H ₆	1.00E+47	1.00E+47	-9.18
Surface Reaction							
<i>2</i>	TMG	+	N(S)	→ TMG(S)	1.16E+05	2.98	0
<i>3</i>	TMG(S)	→	TMG	+ N(S)	1.12E+14	0.55	49675
<i>4</i>	NH ₃	+	TMG(S)	→ TCOM1(S)	3.35E+07	3.33	0
<i>5</i>	TCOM1(S)	→	NH ₃	+ TMG(S)	5.70E+13	-0.161	11922
<i>6</i>	TCOM1(S)	→	3CH ₄	+ GaN(B) + N(S)	1.49E+11	0.609	49675
<i>7</i>	MMG	+	N(S)	→ MMG(S)	1.16E+05	2.98	0
<i>8</i>	MMG(S)	→	MMG	+ N(S)	1.12E+14	0.55	107673
<i>9</i>	NH ₃	+	MMG(S)	→ COMPM1(S)	3.35E+07	3.33	0
<i>10</i>	COMPM1(S)	→	NH ₃	+ MMG(S)	5.70E+13	-0.16	8146
<i>11</i>	COMPM1(S)	→	H ₂	+ GaN(B) + N(S) + CH ₄	3.68E+09	2.05	59610

Figure 2.7: GaN Chemical Pathways for Gas and Surface Reactions

Chapter 3

Simple Computational Model

3.1 Introduction

This chapter will explain the development of the computational model. The computational model will be created using ANSYS Fluent CFD software. Fluent is very simple and efficient at interpreting the elements needed in this computational study. All the governing laws that were mentioned are already embedded into Fluent and it can be changed based on the user's need. Geometry models were created first on a 3-dimensional software called Solidworks. Once the 3D model is complete, it can be imported into ANSYS Fluent for the CFD modeling. Looking at reactor designs, many focus on a vertical impinging type reactor with a rotating susceptor. This reactor style is very common since it yields the best film quality and uniformity. A small experiment model was also constructed to gather experimental data. Validation and various results will be presented in this chapter.

3.2 Simple Computational Model

The model was based on an experimental setup. [23, 24] The setup has a flow guide, and a heated rotating susceptor. To model this, the region between the flow guide and the susceptor is used as the domain of the numerical model. The inlet is 101.6 mm wide, with a total height of 381 mm, the susceptor is 406.4 mm wide and the outlet is 50.8 mm high. To completely capture the effect of rotation, a 3-dimensional model is used. Air is first used to simulate the flow and after that typical carrier gases that industries use. All the dimensions of the experiment model were chosen for a typical manufacturing system. The flow guide above the susceptor plays an important role in

the outflow and this is the overall flow in the system. However, we simplify both the manufacturing and the numerical modelling by using a straight profile so the effect of an arbitrary flow guide profile is not considered. The rotating susceptor has the heating element to provide the thermal energy input. The experimental model has a calculated heat flux of 9,621 W/m², and we employ that input for the numerical model. The 3D model was created on Solidworks and imported into the ANSYS Fluent CFD software.

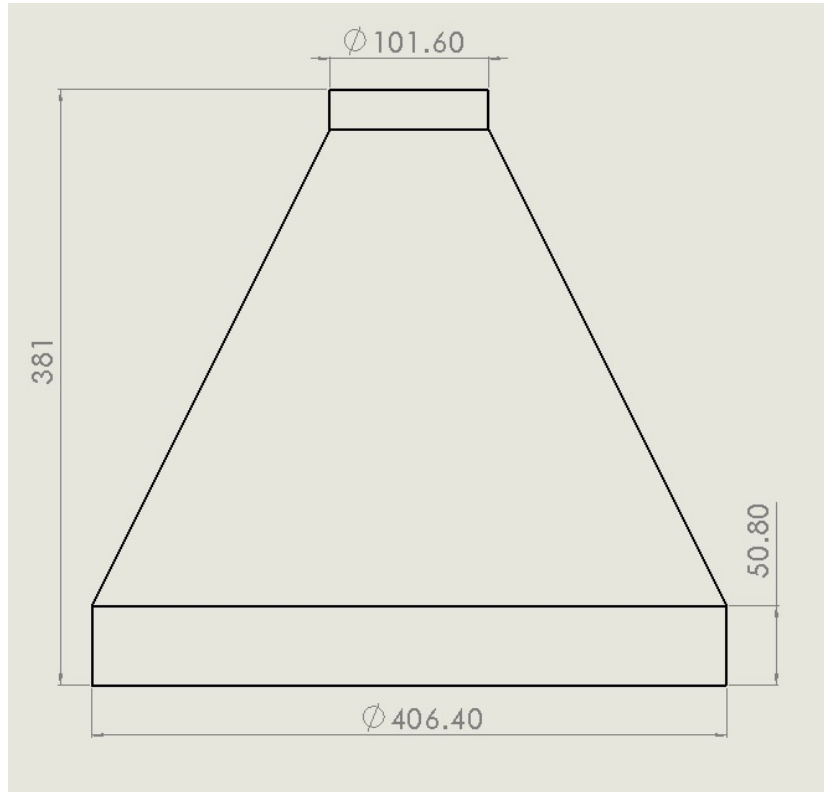


Figure 3.1: 3D geometry model for GaN Simulation

After the model has been imported into Fluent, the next step is to incorporate a mesh into the model. Using the mesh software that is part of Fluent rather than third party meshing software avoids software compatibility issues. The meshing software part of Fluent was designed for CFD applications, and the sizing and refinement can be further adjusted using the custom settings. For this numerical model, fine and smooth meshing algorithm was used with also added mesh size restriction to a maximum of 7.65mm. The total mesh size was 40,155 nodes, and 211,415 tetrahedral elements were

built into this numerical model. It was ensured that its results were grid independent by repeating the calculations over different grids.

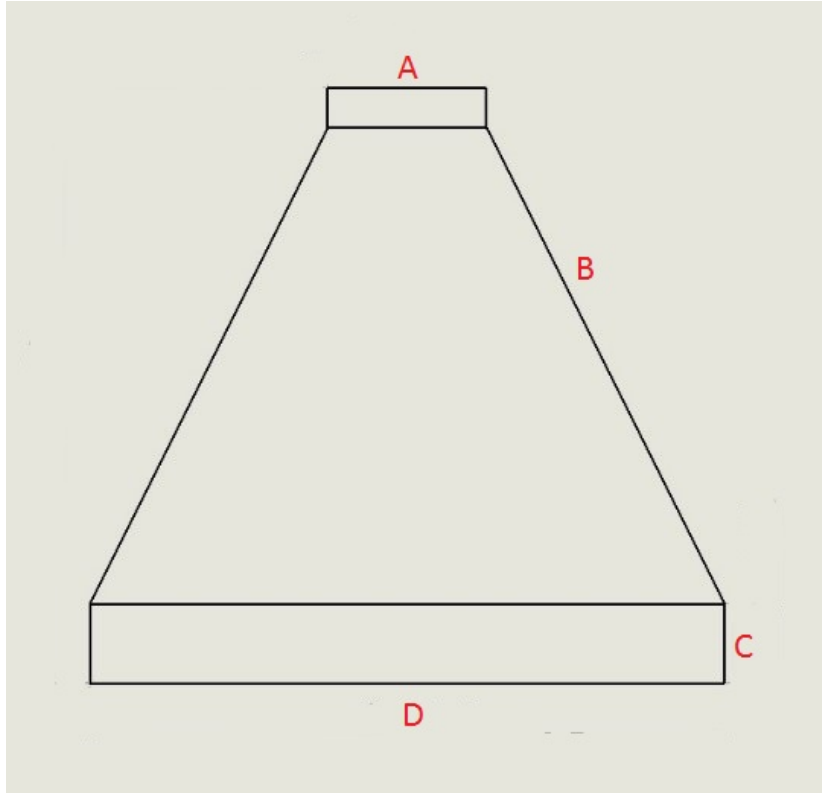


Figure 3.2: Boundary Conditions for 3D Model

The 3D model will be the representation of the volume inside the reactor, and the lines represent the boundary. This method simplified the problem, since we only want the results inside the volume and not beyond the boundary. There are four boundary conditions assigned to the model. The first condition is the inlet, where the flow enters into the chamber denote by A in Fig. 3.2. The inlet is controlled by flow velocity with the constant gas temperature of 300K. Inlet velocities can be changed to study the effect of different inlet velocities. Next will be the wall denote by B in Fig. 3.2. It includes the inlet wall and straight profiled flow guide. This boundary is considered as a mixed condition with heat transfer from natural and forced convection as well as radiation from the heated susceptor. The wall boundary also has the no slip condition. Using an estimation from known sources [8], the total heat transfer coefficient for the air over the

flow guide, denoted by C in Fig. 3.2, is taken to be around 25 W/m²-K. The radiated emissivity for mild steel is set as 0.25 with free stream air temperature of 300K. The susceptor, denoted by D in Fig. 3.2, has a rotating no slip wall condition and has a heat flux input of 962.1 W/m². Meng et al, have shown a comparison between measured temperatures in the CVD reactor with temperatures from the numerical model. The susceptor also has inputs for speed of rotation. Finally the outflow is the circular band around the model. The flow exits on all directions equally.

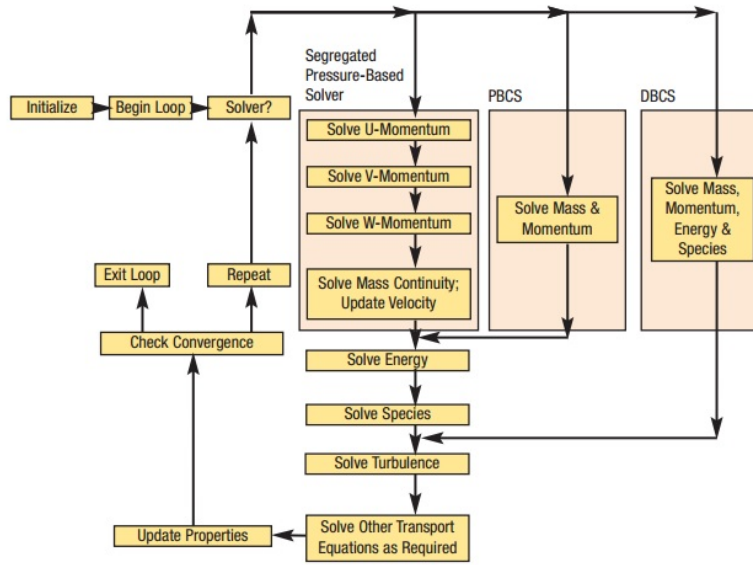


Figure 3.3: Pressure Based Solver Algorithm

In this model, Semi Implicit Method for Pressure Linked Equations or SIMPLE scheme is used to solve the equations. It is a pressure correction Navier Stokes solver. It first takes the boundary conditions, and computes the gradients of velocity and pressure. Next it solves the momentum equation to compute the intermediate velocities. Using the velocities, it computes the uncorrected mass fluxes and then solves the pressure correction term. As the pressure term is updated, it also updates the mass fluxes with the correct values. It then corrects the velocities, from the corrected mass fluxes and pressure. The algorithm repeats until the problem converges. Kelecy describes a pressure based solver [25]...which leads to a more rapid and monotonic convergence rate

and hence faster solution time. Fig. 3.3 shows a diagram of the pressure based solver algorithm.

3.3 Validations

Before analyzing the results, the error and uncertainty of the numerical model must be considered. Errors are known inaccuracy in a measurement or study. Uncertainty is unknown inaccuracy. Repeatability and validation helps decreases ambiguity and increases the confidence of a study or measurement. In numerical studies, there are two main types of errors: round off errors and truncation errors. Round off errors are related to the hardware of the machine. For modern computing, this error is relatively small and the study was done with double precision for more accurate pressure correction. Truncation errors are related to the discretization method of the solver. For SIMPLE scheme, it has a second order error and it is considered small.

Measurement were validated with a computational model. Meng *et al.* created a computational model to simulate the effect of flow characteristics and heat transfer. [26, 27, 28, 29] Meng created a model using the same specification as the experimental value. Taking consideration of energy losses in the system due to conduction, convection and radiative heat loss, we were able to have a very similar trend. The temperature were taken at an arbitrary distance above the surface and we choose to be 0.8mm. First comparison was when there the operating condition has no flow, and no rotation. The results are very similar as shown in Fig. 3.4. The second comparison what when the operating condition for both set to be 50.8mm inlet diameter with a rotational speed of 60 RPM and inlet flow velocity of 1 m/s. Again the result between the computational and experimental model is very similar as shown in Fig. 3.5. There are uncertainties in the flow model. However, experimental result show a 5% to 10% in repeatability, and numerical model shows similar trends compared to experimental results according to Meng *et al.*

Another validation of the model is with the ANSYS Fluent. To make sure the conservation laws and the computational method is correct, a control case was created.

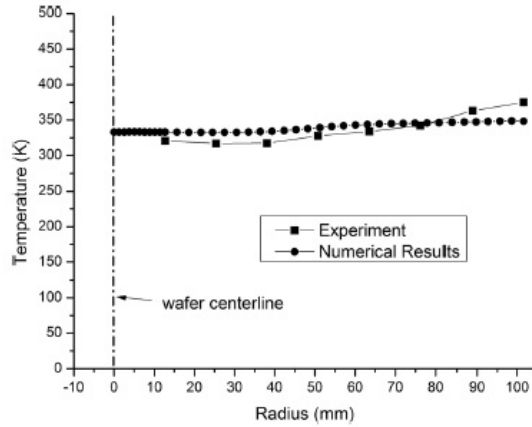


Figure 3.4: Computational and Experimental Temperature Comparison

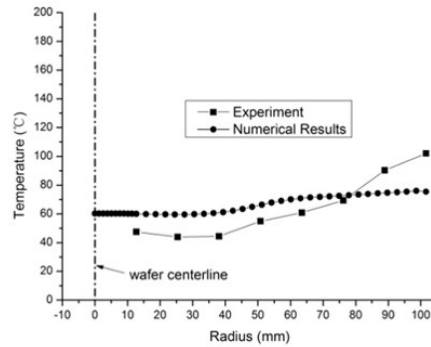


Figure 3.5: Computational and Experimental Temperature Comparison

The control case would be the same model with no fluid flow, and no rotation of the susceptor. This would be a normal convective heat transfer problem where a plate is heat in ambient air. The temperature profile shown indicated that buoyancy effects are import. Higher temperature in the center where the least amount of heat loss, then temperature tapers off to a lower temperature due to the edge where convection, and radiation loss are present. This results matches very well with solution presented in the typical convection heat transfer literatures.

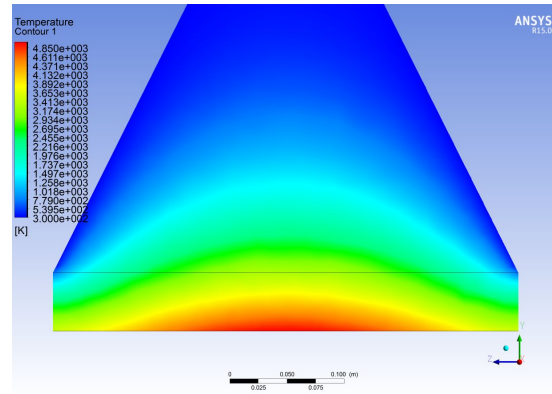


Figure 3.6: ANSYS Fluent Result of Heated Plate in Ambient Air

3.4 Results and Discussion

This section will discuss the results for the simple computational model. The model will only use air as the flow medium. Susceptor would be heated to 1000°C and have a varying rotation from 0 RPM to 600 RPM. The effect of inlet velocity will also be looked at.

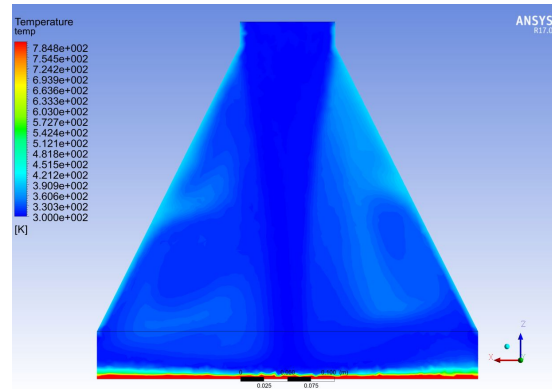


Figure 3.7: ANSYS Fluent Temperature Contour for 0RPM

In Fig. 3.7, the susceptor is at stationary or 0 RPM. At the typical inlet speed of 0.8 m/s, the flow shows disturbances in the reactor. Temperature contour shows light blue in a circular pattern indicating thermal recirculation within the reactor. There are also thermal recirculation above the susceptor near the exit. The thermal boundary

layer above the susceptor are much thinner than when there are no flow as seen in Fig. 3.6.

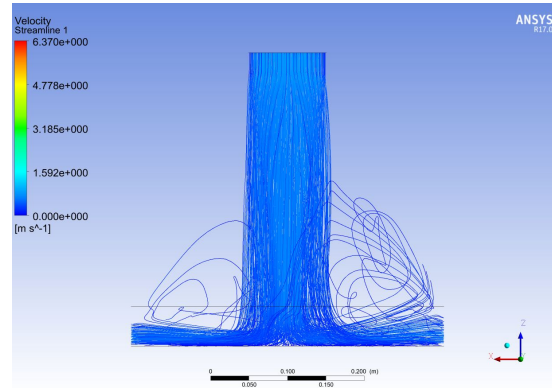


Figure 3.8: ANSYS Fluent Velocity Streamlines for 0RPM

Fig. 3.8 shows the velocity streamlines for the 0 RPM condition. The big circular lines are indications of recirculating flows. The overall physics of the flow matches with standard fluid dynamic conditions. When a flow hits a stagnation point, which is the center of the susceptor, the flow turns and flows out the side exit. The increase in the shades of blue indicating the speed of the flow is decreasing. However there are some light blue regions near the exit which shows higher exit velocity due to recirculation effect. The recirculation energy is driving the flow which in turn increases the speed of the flow near the exit. This increase is very small and does not affect the main bulk of the flow.

Fig. 3.9 shows temperature contours at 300 RPM condition. The thermal gradient on this figure also indicating thermal recirculation inside the reactor. Unlike in the no rotation condition, the driving force in this condition is the rotational energy from the susceptor. The rotation causes flows to pull from both top direction and inward direction. The top direction pull helps the uniformity of the flow across the susceptor while the inward direction pull drives the recirculation area that is above the susceptor. Comparing the 2 conditions, you can clearly see the thermal boundary thickness above the susceptor is thinner at 300RPM. This is a result of improved uniformity due to inducing a rotational effect in the reactor system.

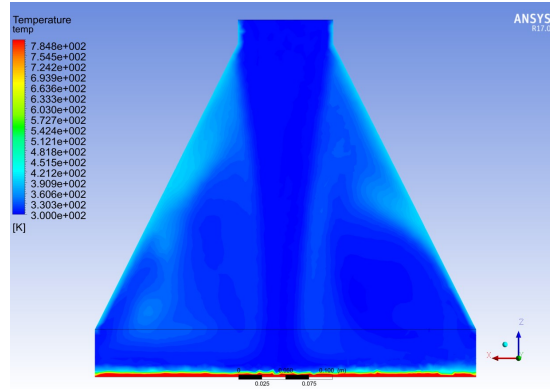


Figure 3.9: ANSYS Fluent Temperature Contour for 300RPM

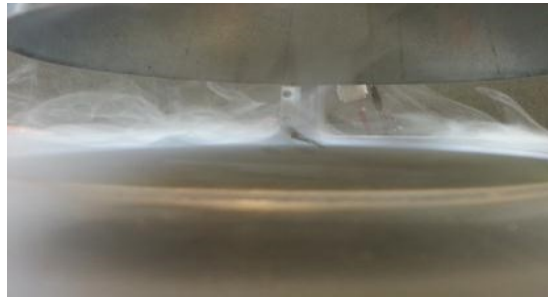


Figure 3.10: Flow Visualization - 0RPM

Fig. 3.10 and Fig. 3.4 are taken from the lab experimental setup using smoke as the visual aid. The smoke for the 0 RPM condition lingers around the susceptor plate while at 300 RPM the smoke is being pulled into an uniform layer above the susceptor plate.

Now looking at the velocity streamlines in Fig. 3.12. The light blue color is consistent from the flow inlet to the outlet, which is different from the previous case where the inlet starts off at light blue and then darkens to a darker blue. The reason agrees with the thermal gradient analysis. The susceptor is driving the recirculation which drives the flow that are exiting. Looking at the center of the susceptor, the flow color is blue indicating lower velocity, and the susceptor near the exit it is red which shows the higher speed of the flow due to the rotation.

The rotational effect greatly improves the surface uniformity of the flow. When the



Figure 3.11: Flow Visualization - 300RPM

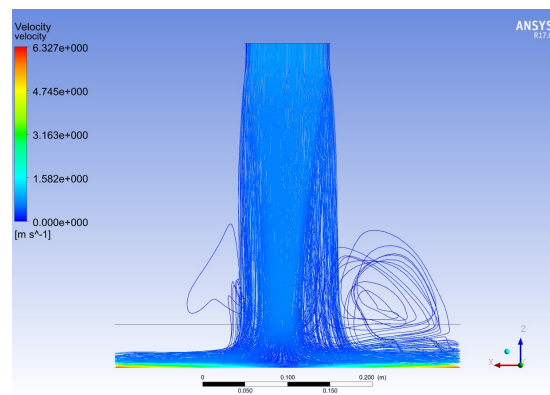


Figure 3.12: ANSYS Fluent Velocity Streamlines for 300RPM

flow is uniform, crystal growth should yield an uniform profile along the substrate and susceptor. Another important conditions is the flow rate. The amount of gases entering the reactor chamber is also critical since the inflow of gases acts like a coolant to the reactor. Too much or too fast of the flow will decreases the overall thermal energy of the system. Fluid particles did not stay long enough inside the chamber to heat up and undergo any chemical reactions which gives you high raw material waste. Too low or too slow of a flow will yield less growth rate or end up having the material overheat and burn off.

Fig. 3.13 is a temperature gradient plot for the same reactor model but a quarter of the original flow speed. Comparing to the previous plots, the light blue region occupies much more area inside the reactor indicating that the overall thermal energy is increasing inside the chamber. This is caused by increase of resident time for the

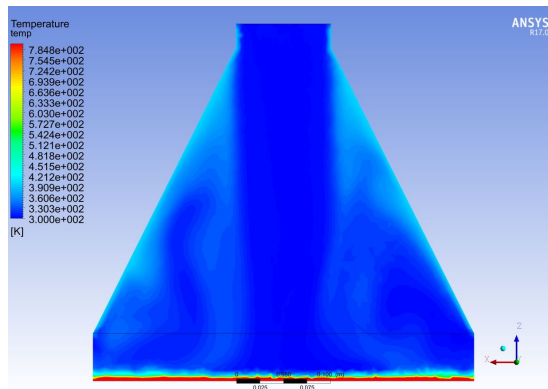


Figure 3.13: ANSYS Fluent Temperature Gradient for 0.25 m/s

fluid particles. Longer the resident time, the more energy the fluid particles will absorb and higher the thermal energy. If the chamber temperature is too high, there would be no material growth. Now let's look at the velocity stream line plot in Fig. 3.14. The recirculation became much more intense due to no momentum in the flow to push the flow out. The rotating susceptor is overpowering the impinging flow causing majority of the flow to rotate with the susceptor. As you can see on the left side of the chamber, there are little to none streamlines that have the direction out towards the exit.

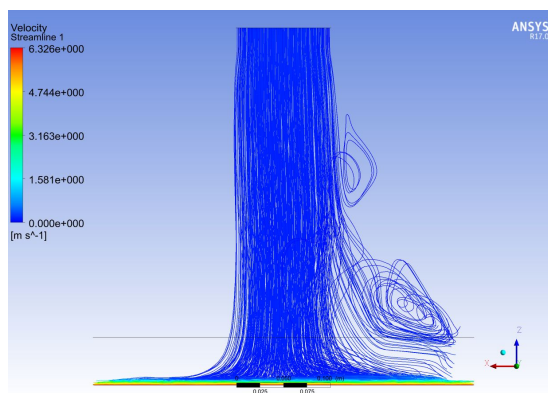


Figure 3.14: ANSYS Fluent Velocity Streamlines for 0.25 m/s

Now looking at inlet speed of twice the original or 2 m/s. In this condition the flow is much more energetic. Doubling the inlet velocity also means that double the mass flow into the reactor chamber. Holding constant pressure, the flow enters and exits much

faster than when it is at 1 m/s. Fig. 3.15 shows the overall thermal gradient inside the reactor, and because the resident time for the fluid particles are much lower, the overall thermal energy is also lower. However, the heated area above the susceptor is very uniform across. Looking at Fig. 3.16, indicating average speed of the flow increase. Recirculation are forming in the cavities between the flow paths and the flow guide, but however, the bulk of the flow are still flowing to the exit. The effect of rotation seems reduce as more stream lines are pointing towards the exits.

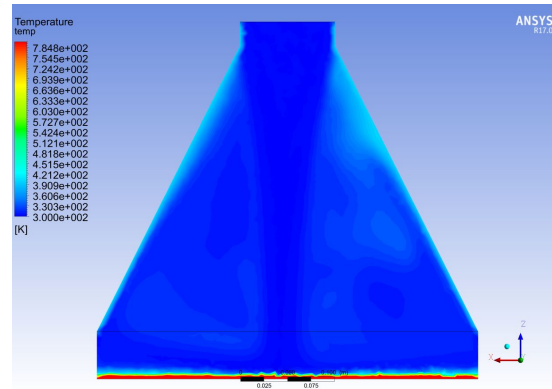


Figure 3.15: ANSYS Fluent Temperature Gradient for 2.00 m/s

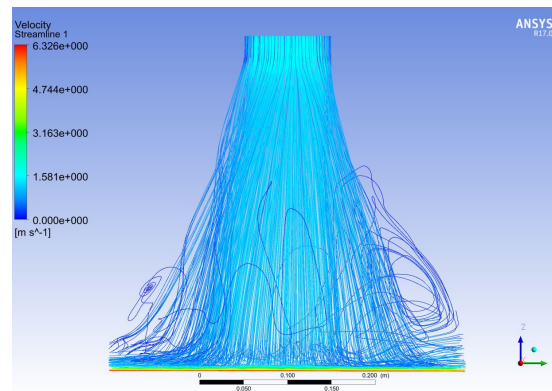


Figure 3.16: ANSYS Fluent Velocity Streamlines for 2.00 m/s

3.5 Conclusion

For this section, we looked at a very simple computational model that shows a CVD reactor with no reactions and air as the fluid medium. Even without the full chemistry model, the problem is very complex. Many variables controls the flow characteristics inside the reactor chamber. The effect of rotation and the effect of inlet velocity sets the overall uniformity and the thermal energy inside the system. Flow speed is very important since too low of a flow speed, buoyancy force will dominates and causes disturbances in heat transfer. When the flow is too high, the average thermal energy is reduced and cause disturbances in the overall flow characteristics. In the next chapter, the effect of different concentrations of chemical gases would be look at.

Chapter 4

Chemical Computational Model without Reaction

4.1 Introduction

In this chapter, the simple computational model will again be used. However, the conditions for the model will be modified to incorporate chemical gas such as Nitrogen, and Hydrogen. Majority of the bulk flow coming in from the inlet are made up of N_2 and H_2 . These are the carrier gases for the GaN CVD reactor. Different concentration of these gases affect the flow characteristic inside the reactor chamber. Both N_2 and H_2 has different molar masses and their reaction to absorbing heat is different compared to air. This part of the study is necessary before simulating the entire chemical model.

4.2 Simple Chemical Model

In this simple chemical model, the use of carrier gases were added to the previous computational model. In a commercial reactor, the reactor chamber usually operates at a low pressure. In order to simulate a real reactor, the computational model pressure will be set to 200 Torr. This pressure condition were taken from the industry CVD reactor. The gases used in the GaN Growth are Nitrogen, Hydrogen and Ammonia. However the bulk percentage of the flow inside the reactor are Nitrogen and Hydrogen, therefore, those are the gases that will be included in this computational study.

To ensure the spatial resolution is suffice for the current model, mesh refinement will be needed. In the previous model, air was used and it was just flowing from the inlet to the outlet. However, for this model, different species of gas will need to be mix and the computational model must have a suffice spatial resolution to capture the fluid flow and the fluid mixing. Ansys Fluent can conveniently increase the grid sizing by

adding a refinement definition. After the refinement, the total nodes is now 72,919 and element count is 409,378. This is a 45% increase for the node counts and 48% increase for the element count. Maximum mesh size is appear to be 0.03 mm and minimum to be 5×10^{-9} m. If the mesh size is as small as a particle size, then Fluent would not able to solve the computational model properly and will cause divergence due to excessive computational errors. Hydrogen atom is to the order of 10^{-12} m and the mesh size is bigger than the particle; therefore, the new impose mesh size is sufficient for this computational study.

Modeling chemical gases require the use of the Species module in Fluent. Once the module is activated, nitrogen and hydrogen can be added to the list of fluids that will be use. Once it is been added, users can adjust the percentage of each species of gas for the computational study. Changing the concentration of the two gases changes the flow characteristic of the flow. In the next section, results of various condition will be presented.

4.3 Results and Discussion

Results of various flow conditions with Nitrogen and Hydrogen will be presented in this section. The result of this section is an important step for the full chemistry model. The amount of each carrier gases used determines how well the precursor and reactant gas mix before chemical reaction occurs. It also model how well it moves the mix gases to the susceptor surface for surface reaction. To show a difference between Air and the use of N_2 and H_2 . The first result will be the use of Air under low pressure condition.

Fig. 4.1 and Fig. 4.2 shows the temperature contours above the heated susceptor, and the flow streamlines when the inlet velocity is set at 0.25 m/s and there is no rotation. As soon as the cool air enters the chamber, the overall thermal energy decreases. Fig. 4.1, shows the temperature distribution right above the susceptor plate. The center is cooler than the edge because the flow is impinging the center area first before the flow turns and exits the chamber as shown in Fig. 4.2. It also shows recirculation caused by the outlet and the wide cone shaped flow guide. As stated before, recirculation

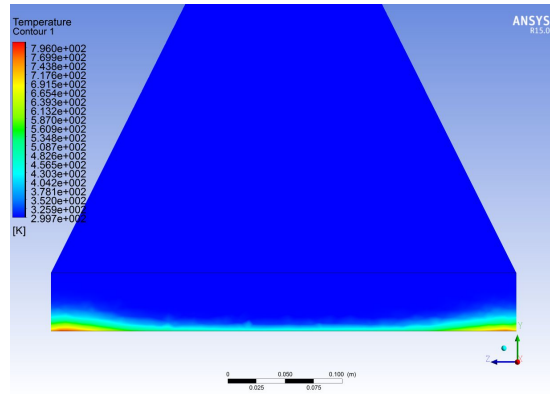


Figure 4.1: ANSYS Fluent Temperature Contour (Air, $V=0.25$ m/s, 60 RPM)

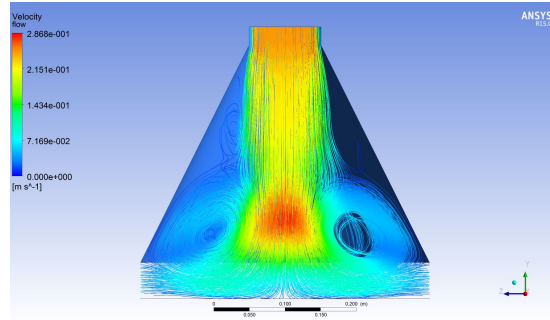


Figure 4.2: ANSYS Fluent Flow Streamline (Air, $V=0.25$ m/s, 60 RPM)

in a CVD reactor causes thermal variations and influences uniformity and deposition. These are the two most critical characteristics in evaluating the performance of the CVD reactor.

Once we turn on the rotational effect, the flow and temperature inside the chamber change again. Fig. 4.3 and 4.4 shows these changes. With just a small rotational speed, the overall characteristics change dramatically. Fig. 4.3 shows the temperature field above the susceptor becomes much more uniform. The overall temperature decreases, as more thermal energy is drawn out of the reaction chamber due to the rotation. Overall flow velocities increase due to centrifugal acceleration and flow streamlines are flatter near the susceptor compared to the no-rotation case. The flow near the edge of the susceptor is being drawn out by the centrifugal effect, hence the high velocity area.

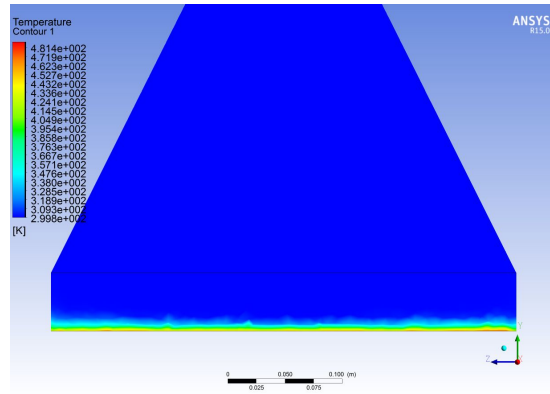


Figure 4.3: ANSYS Fluent Temperature Contour (Air, $V=0.25$ m/s, 60 RPM)

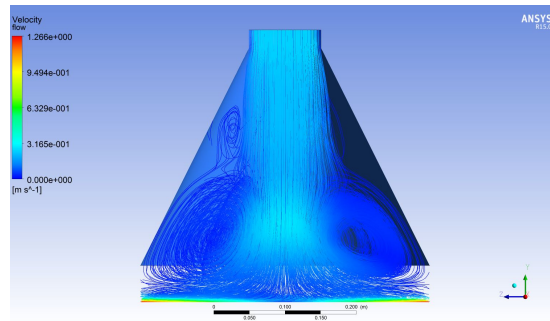


Figure 4.4: ANSYS Fluent Flow Streamline (Air, $V=0.25$ m/s, 60 RPM)

The recirculation increased due to increase in overall fluid velocities, and a second eddy occurs near the top of the flow. This effect causes higher particle residence time inside the chamber. Longer residence time indicates that the molecules are not undergoing reaction and deposition. It causes thermal hotspots where the temperature is too high and precursor gas either turn into unwanted radicals or it burns up completely.

In next set of results, Nitrogen was used as the fluid medium. Nitrogen or N_2 is a carrier gas that many industries use for the CVD process. Since air is 78% Nitrogen, there wont be a drastic change in the temperature and flow characteristic. Fig. 4.5 and Fig. 4.6 show a very similar temperature distribution and flow streamlines, compared to using air as the fluid medium. The overall temperature is higher compared to air, but overall velocities stayed approximately the same for both fluids. Fig. 4.5 also

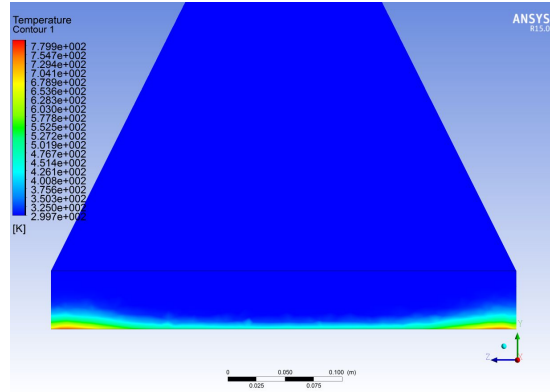


Figure 4.5: ANSYS Fluent Temperature Contour (N_2 , $V=0.25$ m/s, 0 RPM)

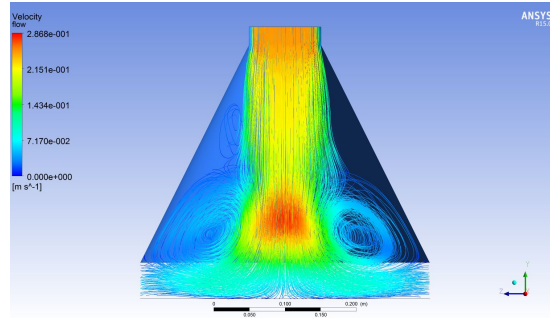


Figure 4.6: ANSYS Fluent Flow Streamline (N_2 , $V=0.25$ m/s, 0 RPM)

shows the increase in temperature as one moves away from the center since the flow is impinging on to the center section of the susceptor. The lack of rotation causes the flow to be recirculated more rather than exiting the reactor. For the next set of results, the rotational effect for Nitrogen will be examined.

Observing Fig. 4.7 and Fig. 4.8, the effect of rotation for Nitrogen as fluid medium is also similar to the air case. Temperature distribution is very similar compared to air. The profiles are very uniform across the susceptor. However there is quite a change in the velocity flow field. Overall velocities are very similar but we do not have the second eddy formation near the top of the chamber comparing to the air case. This indicates the bulk flow carries the gaseous molecules in and out of the chamber, and does not let the molecules linger around to create thermal hot spots. This will improve overall film

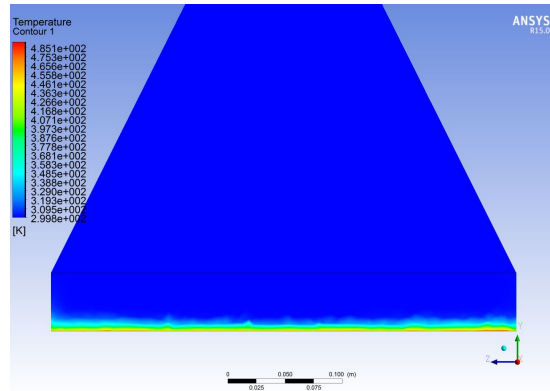


Figure 4.7: ANSYS Fluent Temperature Contour (N_2 , $V=0.25$ m/s, 60 RPM)

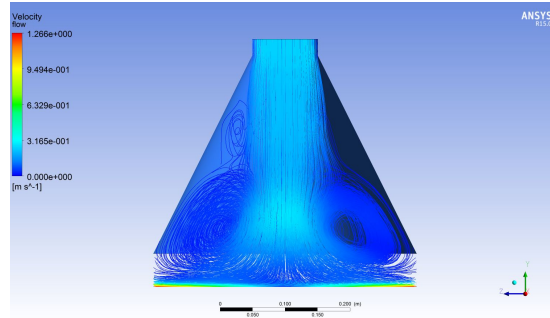


Figure 4.8: ANSYS Fluent Flow Streamline (N_2 , $V=0.25$ m/s, 60 RPM)

quality. The flow lines near the exit are as uniform as compared to air. The effect of rotation does indeed assist in creating uniform and smooth flow from inlet to outlet.

The next step is to evaluate the system when the carrier gas is set to Hydrogen. Unlike Nitrogen and Air, Hydrogen is very light in atomic weight. The tendency to rise is much higher than Nitrogen and Air. Fig. 4.9 and Fig. 4.10 show temperature and velocity profiles for the CVD reactor with hydrogen as fluid medium. Observing the results obtained, the hydrogen case is very different from those for Nitrogen and Air. The temperature profile looks sinusoidal across the susceptor, and the flow is very chaotic. Recirculation eddies are everywhere inside the chamber. Despite of the chaotic thermal and fluid characteristics, Hydrogen is still needed in a GaN growth process by neutralizing other species or radicals. It not only serves as the carrier gas

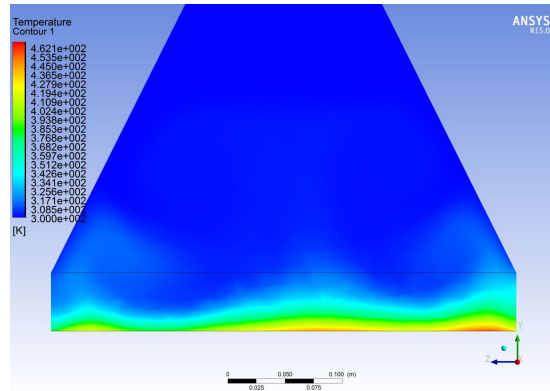


Figure 4.9: ANSYS Fluent Temperature Contour (H_2 , $V=0.25$ m/s, 0 RPM)

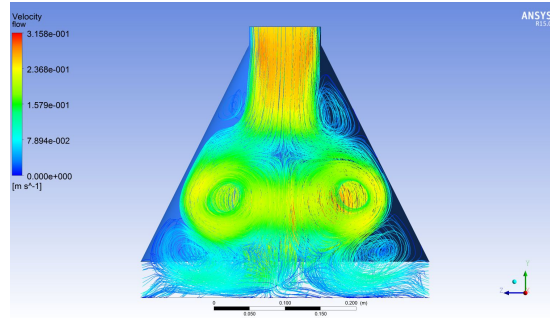


Figure 4.10: ANSYS Fluent Flow Streamline (H_2 , $V=0.25$ m/s, 0 RPM)

but also a gas to enhance GaN film growth. Pearton et al [30] stated that, Hydrogen is a technologically important impurity in growth and doping of GaN films. He also stated that H passivates all the acceptor impurities of Mg, Ca, Zn, and C Therefore precise control of Hydrogen is very important to keep film growth is at its maximum. Even with the effect of rotation at 600 RPM, the Hydrogen still continue to create recirculation effects above the susceptor area, Buoyancy effects near the edge continue to prevent the Hydrogen gas from exiting the chamber. However, using a mixture of Nitrogen and Hydrogen as the carrier gas helps to aid the flow characteristic in the chamber. The flow takes advantage of the heavy nitrogen molecule that will help bring the bulk of the gas in and out of the chamber, while having Hydrogen to aid the crystal growth.

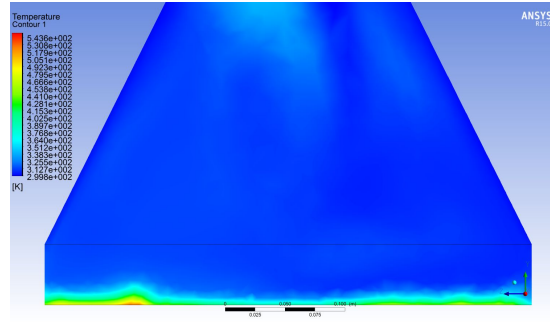


Figure 4.11: ANSYS Fluent Temperature Contour ($N_2=70\%$ $H_2=30\%$, $V=0.25\text{m/s}$, 0 RPM)

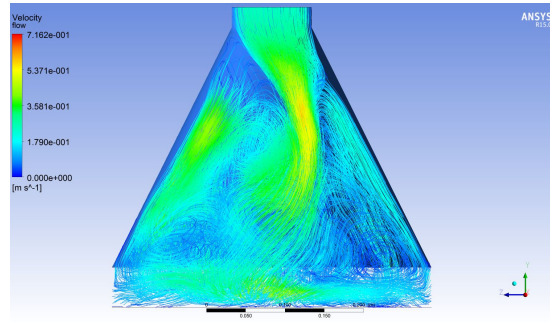


Figure 4.12: ANSYS Fluent Flow Streamline ($N_2=70\%$ $H_2=30\%$, $V=0.25\text{m/s}$, 0 RPM)

Fig. 4.11 and Fig. 4.12 shows the flow and temperature results for the Nitrogen 70% and Hydrogen 30% mixture with 0 RPM. With the 70%/30% Nitrogen-Hydrogen mixture, the temperature profile stabilizes as seen in Fig. 4.11. Comparing Fig. 4.9 and Fig. 4.11, the thermal recirculation around the exit is reduced. This indicates that the flow remains parallel to the plate as the flow exits the chamber and does not have heated gas recirculation back into the chamber. However, looking at Fig. 4.9, we see that temperatures increase in the chamber causing disruption of the incoming flow. Comparing the flow characteristic between Fig 4.10 and Fig. 4.12, it is clearly seen that the amount of recirculation has been reduced, but the intensity increases. Looking at the velocity scale, the flow speed in the recirculation in Fig. 4.12 is increased, indicated by the area of green which correspond to speed approximating 0.358 m/s, while the recirculation speed in Fig. 4.10 remains below the inlet velocity. The increase

in the flow recirculation velocity causes the inlet flow to change and it is no longer flowing perpendicular to the susceptor. Investigating this further, it was found that increasing the inlet flow velocity and increasing the rotation, reduces the recirculation effect even more. Otherwise, the surface deposition will be more distributed and causes non uniform films.

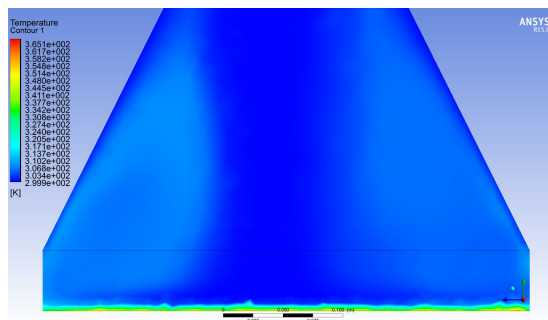


Figure 4.13: ANSYS Fluent Temperature Contour ($N_2=70\%$ $H_2=30\%$, $V=1$ m/s, 600 RPM)

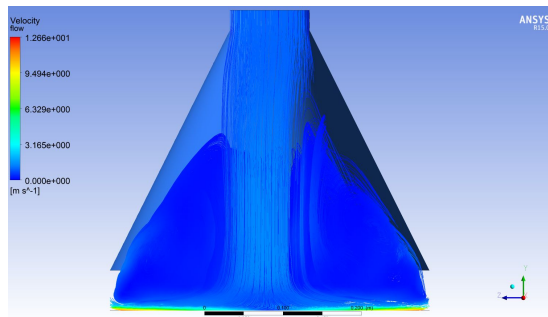


Figure 4.14: ANSYS Fluent Flow Streamline ($N_2=70\%$ $H_2=30\%$, $V=1$ m/s, 600 RPM)

The temperature and flow results shown below has an inlet velocity of 1 m/s with 600RPM susceptor rotation. Observing the results for Fig. 4.13, the temperature distribution is very uniform across the susceptor. Since thin film are on the order of microns, the thickness of the profile is very favorable for chemical reactions near the susceptor. Notice the thermal pockets on either side of the main incoming flow. This is the consequence of the recirculation flow from the bulk flow. However, this increase in thermal energy is not enough to cause chemical reactions in that area compared

to the area near the susceptor. Looking at Fig. 4.14 closely, even though there are big recirculations, the main bulk flow moves smoothly from the inlet to the outlet. Streamlines near the susceptor are parallel indicating that flow are being pulled from the center due to the centrifugal force. It is clearly seen here that even at a higher flow with mixture of light and heavy gases, the effect of rotation will help guide the flow out of the chamber. Even though we see recirculation, the average speed of the recirculation area is low.

4.4 Conclusion

In this chapter, the simple model was developed into a simple chemistry model without the reaction. The purpose of this step is to show the effect of the two carrier gases presented in industry CVD reactors. Different concentrations of the gases yields different flow characteristic inside the reactor. Using an optimal concentration will increase mixing effects and gas delivery; which turns yields a higher growth rate and favorable uniformity.

Chapter 5

Full Chemistry Model

5.1 Introduction

In this chapter, a full chemistry model will be used on the simple reactor model. The full GaN model, both 69 equations and the 11 equations model will be evaluated and validated. Once validated, the 11 equation model will be used for the computational method. A set parameter will be taken from a real CVD GaN reactor. This is to serve as a control conditions. Then 3 of the parameters will be modified and computed. A detail breakdown of the modified condition will be present in the later section. In addition to the analysis of the fluid flow characteristic and heat transfer inside the reactor, GaN growth rate and the characteristic of uniformity will also be look at.

5.2 Full Chemistry Model

The full chemistry model, adapted from Sengupta, consist of 69 chemical reactions pathways that TMGa undergo reaction with ammonia to get gallium nitride deposition. Many study has been done to simulate the 69 equation model such as Meng. However, Hu et al, was able to reduce the model down to a 11 equations model. Decreasing the overall setup and computational time. A validation case will be presented between the 69 equation model and 11 equation model. The condition parameter are set as follow: Inlet Velocity at 6 m/s, Temperature at 1000K, Pressure at 200 Torr, Rotational Speed at 600 RPM, and V/III ratio set at 2000.

In Meng et al results are presented for the simple model geometry with the 69 equation model. The model is run on CFD-ACE rather than Fluent Ansys. However the results are very similar. Temperature gradient for the Meng et al case is shown in

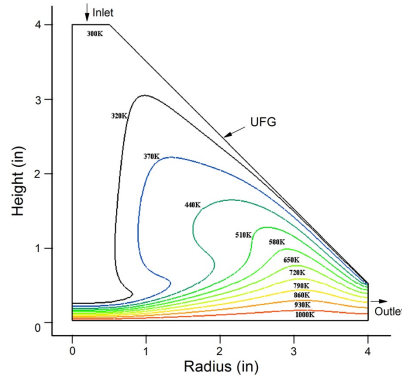


Figure 5.1: Temperature Contour Diagram from Meng *et al.*

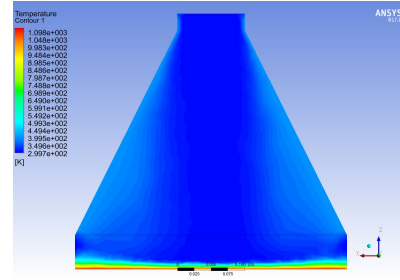


Figure 5.2: Temperature Contour Diagram from the 11 Eqn Model

Fig. 5.1 and Fluent 11 equation model case in Fig. 5.2. Temperature contour shows near the exit, the thermal boundary layer shows very thin and uniform at the center area of the susceptor. The boundary layer thickness also increases as it move toward the exits. The gradient change is also very similar.

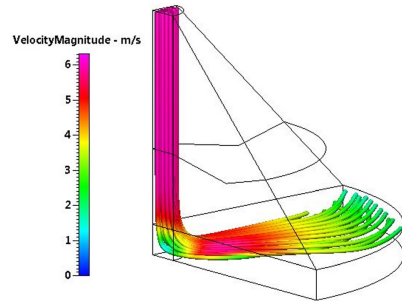


Figure 5.3: Velocity Streamline Diagram from Meng *et al.*

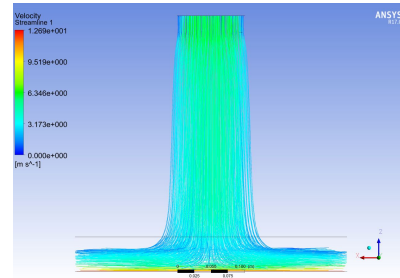
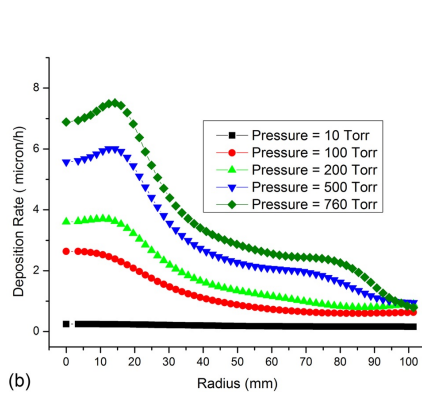


Figure 5.4: Velocity Streamline Diagram from the 11 Eqn Model

Looking at the Meng *et al* velocity streamlines for Fig. 5.3 and the fluent model in Fig. 5.4 shows similarity. Both has a straight and laminar inlet flow, then the flow turn at a 90 degree angle towards the exit. However the fluent model also took effect from the rotation, therefore the flow near the susceptor seems higher because rotational speed is high. The strongest comparison is the growth rate between the 69 and 11 equation models. In Fig. 5.5 shows various growth conditions for different Pressure. Looking at 200 Torr case, the lines start around 3.5 microns per hour, and peaks at around 4 microns per hour then decreases to less than 1 micron near the exit. In Fig. 5.6, near the center it's starts at around 4 microns per hour then increase to around 5 microns

per hours and then decrease to around 1 microns per hour.



(b)

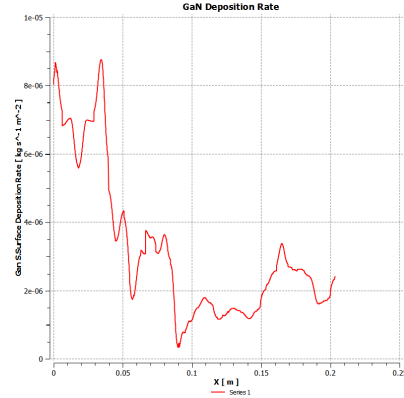


Figure 5.5: Deposition Growth Chart from Meng et al. Figure 5.6: Deposition Growth Chart from the 11 Eqn Model

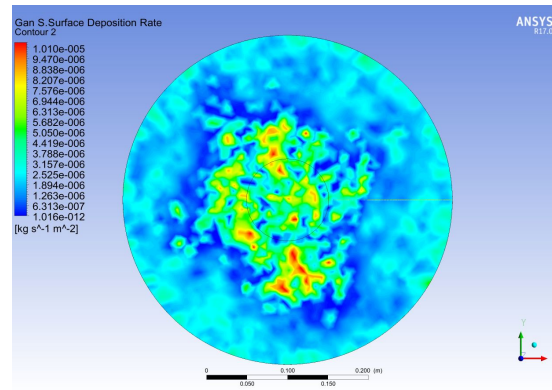


Figure 5.7: Deposition Contour Map from the 11 Eqn Model

Hu et al paper can also be used to validate the models. The 11 equation model was adapted from them. According to Hu et al, the 11 equation model named new model was compared to the original 69 equation model and experimental results. In Fig. 5.8, the growth rate was within 10% of the experimental results. This validation will allow the research to move forward with the 11 equation model. Growth rate will be on the low side, however, the time it takes to setup and compute the results are more favorable.

In the next section, a controlled condition will be presented first. Results will be analyze and discuss. Then various modification to the operating parameter will be

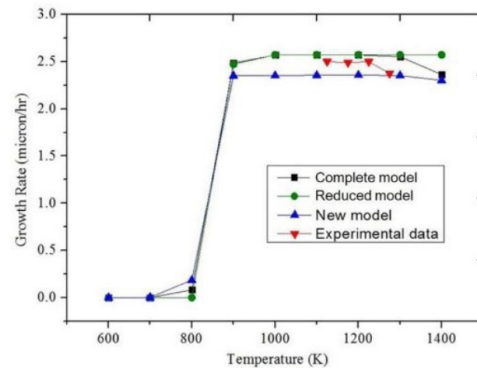


Figure 5.8: Model Comparison. Adapted from Hu et al.

change to simulate and understand the effects to heat transfer and the flow characteristic in the reactor. Most importantly, how the changed in condition does changes for the deposition rate and the uniformity.

5.3 Results and Discussion

A controlled operating condition are adapted from a small industry CVD reactor. This set of conditions are used for simulation purposes and the geometry of the two reactors are very different. The simple cone geometry will be used in this study as well. Fig. 5.9 shows the breakdown of the control conditions. The flow composition are 25.5% for Nitrogen, 34.8% for Hydrogen, 39.6% for Ammonia and 0.1% for TMGa. As stated in the previous chapter, Nitrogen and Hydrogen takes up 60% of the total flow. Reactor pressure has been set at 140 Torr, rotational speed at 60 RPM, and an inlet velocity is currently set at 0.06 m/s Effects of pressure, inlet velocity and rotational speed would be analyze.

Reactor Conditions		Flow Composition	
Mass Flow Rate	3.18x10 ⁻⁵ kg/s	Nitrogen	25.50%
Inlet Velocity	0.06 m/s	Hydrogen	34.80%
Pressure	140 Torr	Ammonia	39.60%
Rotation Speed	60 RPM	TMGa	0.10%
Susceptor Temperature	1273 K		

Figure 5.9: ANSYS Fluent Reactor Conditions - Control

The control condition are tuned for the industry CVD reactor geometry and using the same condition in this model would not be a good condition to grow GaN. The following figures will shows the results that supports the claim. Using the 11 equation model, computational results are given as follow. Fig. 5.10 shows the temperature contour. In this figure, the yellow contours indicates that thermal recirculation is occurring due to the flow and buoyancy presented in the system. The two areas where the recirculation occurs are off centered due to flow impinging at the center. One rotates left and one rotated right towards the exit. Thermal recirculation causes hot spots where the molecule could burn up when it is exposed to the high temperature for extend period of time or high residence time. Molecule resident time should be the time it takes to flow from the inlet, absorb energy for reaction, undergo reaction, and then exit the chamber. Hanging around inside the reactor cause the molecule to absorb too much heat and it would just break down.

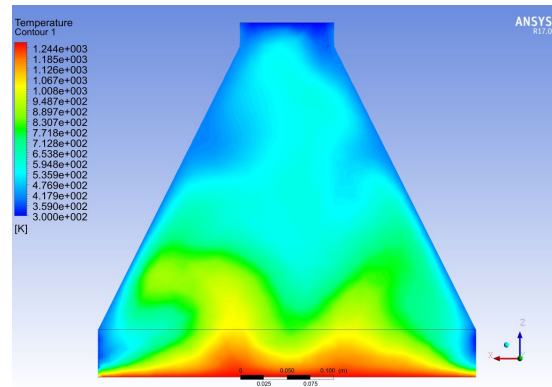


Figure 5.10: Temperature Contour - Control

Fig. 5.11 shows the flow streamlines of the 11 equation model. As seen in the figure, the flow is very chaotic. There are recirculation eddys everywhere, and nothing resemble a laminar flow. The reason for this results is the low inlet velocity of 0.06 m/s and the low susceptor speed of 60 RPM. The buoyancy forces dominates and drive the flow to turn. Fig. 5.10 shows thermal field from the susceptor, as it raises it turn like a thermal plume and that causes the flow to become chaotic. Increasing inlet flow velocity and increasing susceptor rotation would dominate the buoyancy force and improve overall

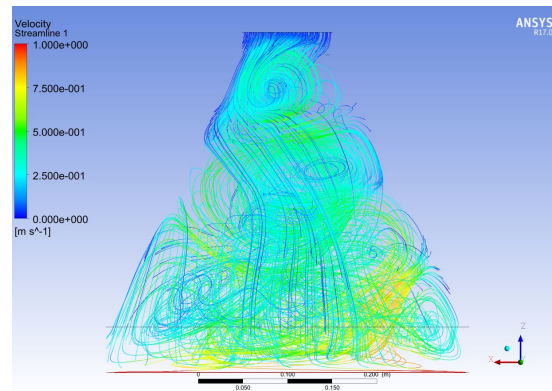


Figure 5.11: Flow Streamlines - Control

flow characteristic.

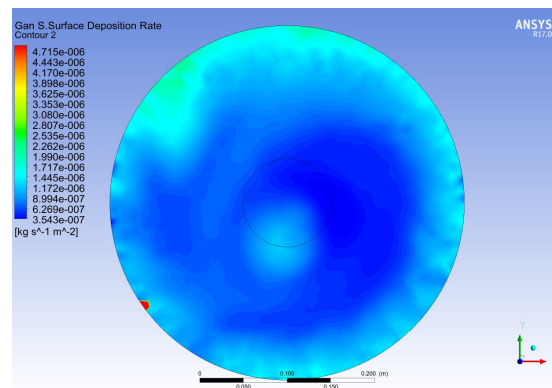


Figure 5.12: Growth Contours - Control

Fig. 5.12 shows the growth or deposition rate contour. The average deposition rate was around 2.1×10^{-6} kg/s·m² or 1.26 microns per hour. Using the same condition in the small industry CVD reactor would yield around 3-4 microns per hour. The contour would be much more uniform. The contours resemble a twist indicating the reaction occurs while it was turning. This is caused by the chaotic flow. If the flow was outward instead of twirling motion, the deposition would be much more uniform and would even deposit at a higher rate.

5.3.1 Effect of Pressure

Pressure inside the system is an important conditions that operator need to pay attention to. In a real CVD reactor, the lower the operating pressure is the higher the purity of the crystal is but it give a low deposition rate. At atmospheric pressures, growth rate are high, but the crystal will prone to have impurities. Even though lower pressure has purity advantage, having it grown at lower pressure also increases the production cost. Lower the pressure, the longer it will takes to have the pump out the atmosphere inside the reactor chamber, and also the bigger the process pump to maintain the pressure while the system is running.

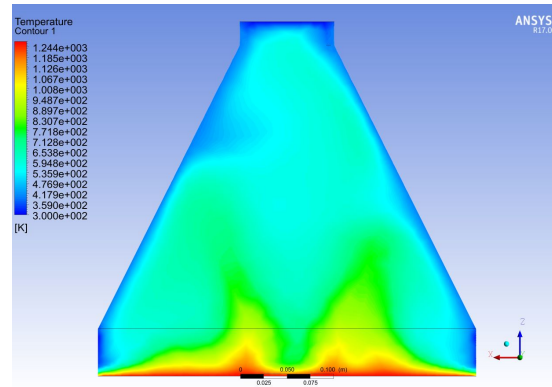


Figure 5.13: Temperature Contours - Effect of Pressure

In this section, pressure will increase from 140 Torr to 200 Torr. Any changes in pressure also changes the temperature. If everything is held constant, temperature will increase if the pressure increases. In Fig. 5.13, the light blue and green area covered most of the reactor chamber, while in Fig. 5.10 there are still some blue present in some of the area near the inlet. The plume like area shows the buoyancy is still dominates and thermal recirculation is driven by that force. Overall thermal uniformity is very poor, and it will affect the overall growth uniformity results.

Increasing pressure also influence the flow characteristic in the system. In Fig. 5.14 shows streamlines does not seem to be improve, however the larger recirculation has dissipated into smaller ones and there are some resemblance of laminar flow that flow from the inlet to outlet. However, it is still considered a very chaotic or turbulent flow.

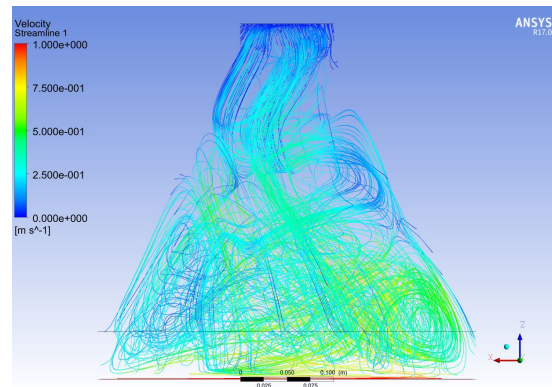


Figure 5.14: Flow Streamlines - Effect of Pressure

This type of flow will also cause uniformity problems in the growth results.

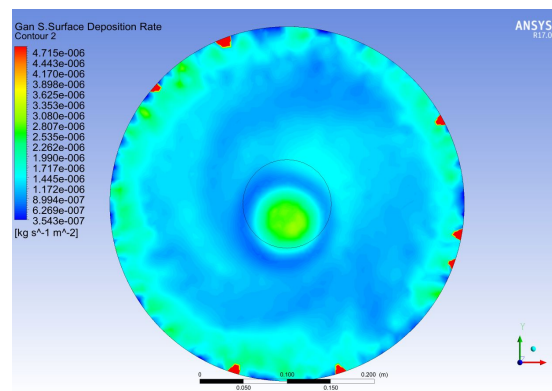


Figure 5.15: Growth Contours - Effect of Pressure

For this case, Fig. 5.15 shows improvement from Fig. 5.12. Keeping the scale the same, the total deposition increase. Dark green center indicate fluid flow is staying in the center and not pushing the flow out to the exit. Uniformity is not the best. With the average low point to be around 0.68 microns per hours and high point located near the center to be 1.87 microns per hour. The overall average deposition rate was increased to 2.23×10^{-6} kg/s-m² or 1.31 microns per hour. Not a very high increase in deposition as an average but the coverage was certainly improve.

5.3.2 Effect of Inlet Velocity

Another important operating condition is the inlet flow velocity. As mentioned earlier, the control condition's inlet velocity was too low for this model, and hence the reason why the buoyancy force dominate. By increasing the inlet velocity, the overall bulk flow momentum should increase so the flow could be push toward the exit rather than getting recirculated by the buoyancy forces. The inlet flow velocity will increase a factor of 10 from 0.06 m/s to 0.6 m/s.

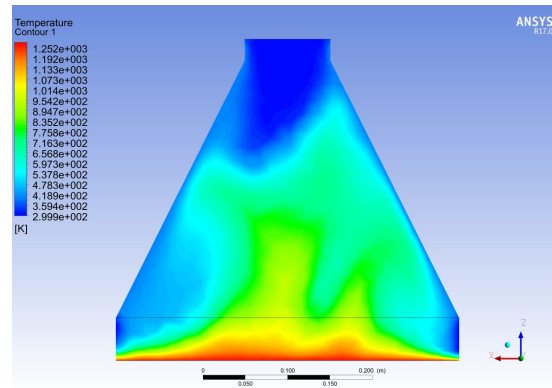


Figure 5.16: Temperature Contours - Effect of Inlet Velocity

In this model, Fig. 5.16 shows the thermal boundary layers are not very uniform. However, it is an improvement compared to the control condition in Fig. 5.10. The cooler bulk flow is now penetrating further into the system and cooling some of the surrounding area. Recirculation is still present however the size of the thermal recirculation has been reduced. The thermal boundary layer also showed an improvement since the buoyancy effect might have been reduced based on the smaller thermal gradient raising from the susceptor.

In Fig. 5.17 shows characteristic of laminar flow, however there are still more flow recirculating than exiting. The higher velocity denote in red shows flows are circulating at high speed. The combination of the momentum from the incoming bulk flows and the buoyancy force are driving up the velocity speed in the center. For the flow to exit, a higher inlet speed might be required to push the flow out the system. There is some improvement however, it is not noticeable where it can consider a laminar flow.

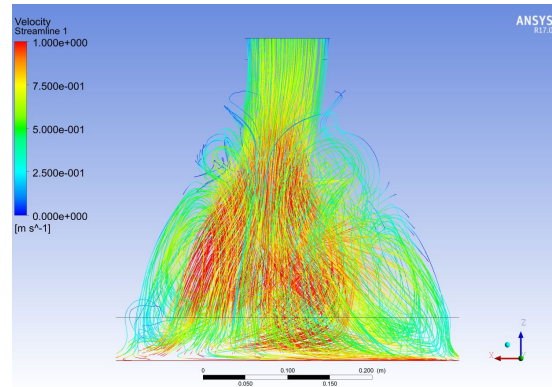


Figure 5.17: Flow Streamlines - Effect of Inlet Velocity

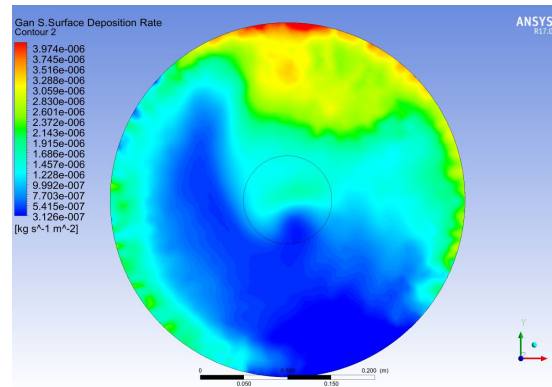


Figure 5.18: Growth Contours - Effect of Inlet Velocity

In Fig. 5.18 shows the deposition rate on the susceptor. Recirculation flow caused the great uneven growth. In Fig. 5.17, the recirculation flow indicated in red are off centered. This is the corresponding deposition rate in Fig. 5.18, where the recirculation flow deposited more and the area with the least flow deposit less. Overall deposition rate is around 1.91×10^{-6} kg/s-m² or 1.12 microns per hour which is an decrease from the original control case. Highest point to be average of 2.11 microns per hours and the low point to be average of 0.40 microns per hours indicating a very poor uniformity across the susceptor.

5.3.3 Effect of Susceptor Rotation Speed

The effect of rotational speed was analyzed for this section. Most modern CVD reactors has some rotating mechanism that is built into the geometry design to improve flow uniformity from inlet to outlet. There are articles that goes in-depth study about the uniformity improvement in a rotational flow reactor. So how does it improve the deposition rate when rotational speed is changed? In the controlled case, the rotational speed was set to 60 RPM and it appears to be very slow. The rotational speed was not high enough to drive the effect of rotational forces to overcome the buoyancy forces and it created chaotic flow and temperature profile in the system. In this section, rotational speed is increased to 300 RPM. Temperature, streamlines and the growth rate will be analyzed to determine if the rotational forces helps with deposition rate and the uniformity.

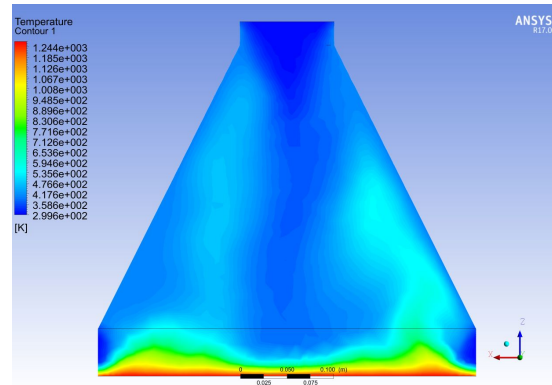


Figure 5.19: Temperature Contours - Effect of Rotation

In Fig. 5.19, the increased in susceptor rotation help pull the flow from the inlet. This is indicated by the darker blue in the middle of the reactor system. Recirculation on the outer part is result from the higher susceptor rotation speed. The thermal plume is now occurs on the outer part of the susceptor which shows that buoyancy effect might be overcome by the rotational effect. This operating condition change improves thermal boundary layer the most. With a more uniform thermal boundary layer, reaction would occurs where it should be occurring, near the susceptor area.

In Fig. 5.20, the flow enters the reactor chamber and then starts to twirl around

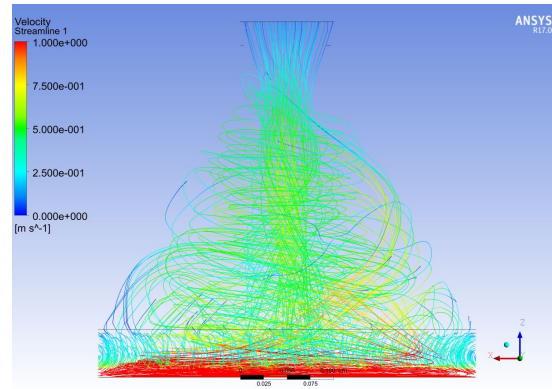


Figure 5.20: Flow Streamlines - Effect of Rotation

because of the susceptor rotation. The main bulk flow resemble a laminar flow where in the previous conditions, this type of straight flow was not seen. Once the flow enters and reaches to the susceptor, the flow get spun around. There are streamlines where it show the flow does make it out of the reactor chamber.

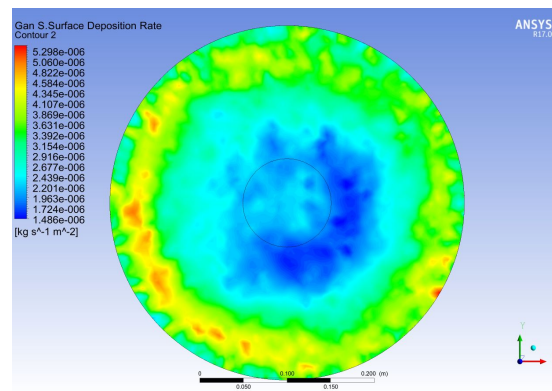


Figure 5.21: Growth Contours - Effect of Rotation

Even with the original 0.06m/s inlet velocity, the rotation effect plays a very important role to growth uniformity. In Fig. 5.21 shows a more favorable deposition and uniformity results. There is a noticeable amount of green in the contour which indicate some uniformity. The yellow are from the revolving flow when the bulk flow is being spun around while the fluid particles has a longer resident time yielding higher deposition rate. The average deposition is measured to be 2.4×10^{-6} kg/s-m² or 1.40

microns per hour. The high area shown in yellow measured 2.63 microns per hour and the low area shown in blue measure around 1.05 microns per hour. The uniformity is much more favorable; however, it is far from industry standard.

5.3.4 Effect of V/III Ratio

Lastly, the effect of V/III ratio is analyzed. V/III ratios is the total group V molar flow rate over total group III molar flow rate. For GaN growth, group V material would be ammonia and group III material would be TMGa. The V/III play a very important role to the growth rates. Low V/III ratio indicates that Ammonia is low or TMGa is high. More TMGa means more of the TMGa will react with Ammonia to yield GaN. High V/III ratios indicates that Ammonia is high or TMGa is low. Higher the V/III ratios the lower the growth rates.

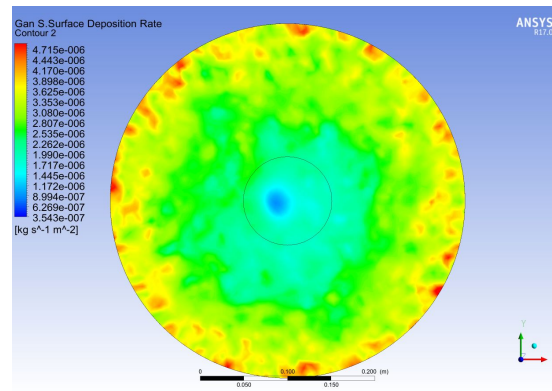


Figure 5.22: Growth Contours - Effect of Low V/III Ratio

In this comparison, Fig. 5.22 has a low V/III ratio and Fig. 5.23 has a high V/III. Keeping all other parameters constant. Fig. 5.22 shows an average of 2.11 microns per hour and Fig. 5.23 shows an average of 1.45 microns per hour. The lower V/III ratio yields a higher deposition because there are more group III tmga to reacts to Ammonia. A very low V/III number indicates a very high concentration on TMGa, and the growth depends on the reactor capability. Some of unreacted TMGa may exit the reactor chamber, if there are not enough thermal energy for chemicial reaction to occur. However V/III increases with the same temperature, not only the growth rates

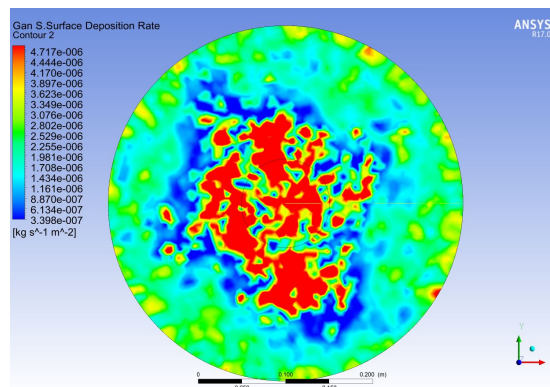


Figure 5.23: Growth Contours - Effect of High V/III Ratio

goes down, but also the growth patterns also changes. Fig. 5.22 shows a smooth growth even though it is not uniform. Fig. 5.23 shows growth in various polygon shapes. These are island growth that occurs when temperature is too high for the corresponding high V/III ratio. These are structural defects that will impact the crystal strength and quality.

5.4 Conclusion

This chapter shows the computational results for the full chemistry model. The chemistry model simulate the chemical reactions between TMGa and Ammonia to get Gallium Nitride deposition results in addition to the fluid and heat transfer results. Chamber pressure, inlet velocity and susceptor rotational speed were chosen to be those operating parameters and the results are very interesting. Increasing pressure will allow more deposition, however it increases chamber temperature and induce more buoyancy effect into the system. Increasing the inlet velocity will help with overall chamber cooling and help drive the flow out of the reactor but it can lead to flow recirculation. Increasing susceptor rotational speed help with the uniformity of the flow and thermal boundary layers but may causes a the flow to twirl around inside the reactor. Lastly, the V/III ratios can predict the growth rate. The lower the V/III numbers the higher the growth rate. However, it will be limited to the reactor capability. There are certain parameter combinations that will give a favorable results and these combination can be

found using optimization techniques.

Chapter 6

Practical Chemical Vapor Deposition Reactors

6.1 Introduction

CVD process was explained in detail earlier, however there are more to the process itself. There are many components that are required to operate the reactors. In the simple chemical vapor deposition reactor model, the system were simplified down to the reactor chamber; however, there are many subsystems that supports the main reactor for everything to run. In this chapter, a closer look into an actual practical chemical vapor deposition reactor system. In addition, a similar model was created to model the practical chemical vapor deposition reactor. Various conditions were simulated and experimental results from the actual reactor was compared and analysis. Actual growth data are recorded on the practical reactor, and image of the gallium nitride samples were taken for each conditions. Hu et al [31] recently attempt the same experimental comparison.

6.2 Practical CVD Reactor

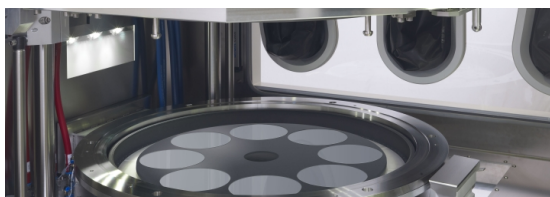


Figure 6.1: Modern Chemical Vapor Deposition Reactors. Source: AIXTRON

In practical chemical vapor deposition reactor system, there are many subsystems that supports the main reactor. These subsystem are the gas supply system, vacuum

system, rotational system, heater system, cooling system, electronic control system and lastly the reactor itself. All these subsystem is supports the main reactor, so optimal growth conditions are meet. Obtaining Optimal growth of gallium nitride also require the use of computers and electronics to controls all the concentrations and flow rates, internal and heater temperatures, internal pressures, susceptor rotation speeds, and cooling of the reactor to prevent from overheating. The electronics also monitors growth thickness and uniformity by the use of non-intrusive laser measurement systems. Detail breakdown of each subcomponent will follow.

6.2.1 CVD Environment

Gallium nitride, in general, is a type of semiconductor. Extreme care is implemented to ensure that the GaN crystal samples are kept in the cleanest and purest conditions. To achieve that, enclosures are to shield from the environments are necessary, especially during pre-growth preparation since dust and other particles can contaminate the samples. Clean rooms are usually where semiconductors reactors are kept to shield from external environments. Level of cleanliest are measured by the amount of maximum particles in a cubic feet. As shown in Fig. 6.2, each class categorized how particles-free the clean rooms are. Lower the class numbers, the higher the cost to operate.

Class	maximum particles/ft ³					ISO equivalent
	≥0.1 μm	≥0.2 μm	≥0.3 μm	≥0.5 μm	≥5 μm	
1	35	7.5	3	1	0.007	ISO 3
10	350	75	30	10	0.07	ISO 4
100	3,500	750	300	100	0.7	ISO 5
1,000	35,000	7,500	3000	1,000	7	ISO 6
10,000	350,000	75,000	30,000	10,000	70	ISO 7
100,000	3.5 × 10 ⁶	750,000	300,000	100,000	700	ISO 8

Figure 6.2: Clean Room Class Chart

Clean rooms are shielding for external environments. The chemical vapor deposition system also require shielding from other chemical environments such as air. Atmospheric Air has contains 78% Nitrogen, 21% Oxygen, 1% Argon, and trace of other gases such as carbon dioxide, Neon, Helium, Methane and water vapors. To ensure

growth are contaminant free, inert gas are used to surround the reactor systems. This is done by the use of a glove box. Inert gas does not reacts to other chemical creating a safe environment for pre-growth preparations and growing stages. Due to natural abundance of Nitrogen in the atmosphere, Purified Nitrogen is the preferred use as the inert gas medium. Using dry Nitrogen purge or flow can reduce dew point to around -94F, creating a dry conditions at normal room temperature.

6.2.2 Vacuum System



Figure 6.3: Vacuum Process Pump

The vacuum system is there to make sure the entire CVD reactor system is under specific pressures. The system consist of a process pump and vacuum tubings into the reactor, glove box and transfer chamber. Process pump is shown in Fig. 6.3. The glove box are kept at higher pressure than atmospheric to ensure contaminates, if any, can flow when the Nitrogen purges and the vacuum pump takes it away. The vacuum pump also maintains the pressure within the reactors. It is the main flow driver for the reactor, and it also removes the gas waste from the reactor. Lastly, the vacuum pump controls and maintains an area where items are transfer between outside environment and inside the glove box. When an item need to be inside the glove box, the vacuum

pump takes out all the atmospheric air and fills it with Nitrogen to match the condition inside of the glove box.

6.2.3 Heater System



Figure 6.4: Heater Coils used for CVD Applications

The heater system is the main energy provider for the reactors. As stated previously, CVD is a heat activated process and the heater system controls and maintains the internal reactor temperature. There are many ways to heat the reactors such as microwave heating, induction heating, and resistive heating. With proper design, internal reactor can reach to a temperature of more than 1600C. The heater system are powered by either alternating current or direct current depending on the heating method. For this thesis, resistive heating is used, and it is easily match to the computational model. Resistive heater coils glows and release high energy to the susceptor area by the use of DC power. The powers are supply and control by commercial high voltage DC power supply units that converts the facility AC to DC. Fig. 6.4 shows a typical heater coil used in resistive heating for the CVD application.

6.2.4 Cooling System

The heater system provides energy to the systems; however, to withdrawal of energy is also require to add additional level of control to the internal temperature. Cooling



Figure 6.5: Chill Water System used for CVD Applications

system helps maintain internal temperature stability as well as cool down internal temperature rapidly. This system consist of water chiller and tubing to supply chilled water to the area where it needs cooling. Water passage can be built internally within the reactor walls for the internal cooling. The water chiller unit must provide a consistent high flow rate at low water temperature to control and maintain temperature during growth and cool down. Overheating will damage various reactor systems and as well as the crystal samples.

6.2.5 Rotational Drive System

In the recent CVD reactor designs, many companies include a rotational susceptors into their model. The rotational effect provide control over the uniformity of crystal growth and it became a necessary condition for the industry. The rotating susceptor can be achieved in various ways. The first way is a direct drive. The servo motor is directly attach to the spindle that the susceptor rest on. Another way is by belt driven. Belt drive utilize drive ratios to reduce rotational speed of the servo motor. If a 1:4 ratio is used, a 300 RPM on the susceptor can be achieve by 75RPM on the motor. Final drive system is similar to the belt drive, but it uses gears. Many companies created creative designs such as planetary rotational susceptors using the gear drive. The main susceptor carrier would rotate clockwise, while the small substrate susceptor would rotate counter clockwise motion. This method can help improve uniformity a bit more since the most outer substrate are getting more reactive products for crystal growth.



Figure 6.6: Rotating Susceptor CVD Reactor. Source: AIXTRON

6.2.6 Gas Supply System

The gas supply system is a very extensive network of flow controlling devices, and gas tubing. Its job is to route various gases into the reactors. The mass flow controller device precisely measure the amount of gas it would allow to pass through. In a typical mass flow controller, it gives the specific gas that the device controls and the maximum amount of flow rate. The flow rate is measured in standard cubic centimeter per minute (SCCM) or standard liters per minute (SLM). To properly use the mass flow controller, the flowing gas must be in gas or vapor form. Standard TMGa is in liquid form and a bubbler is required to convert the liquid form into vapor form. The device consist of a close storage medium for the liquid with an inlet and outlet for the Nitrogen carrier gas. The entire storage medium submerse in a heated bath and when the nitrogen gases enters and exit the storage medium, it carries the vaporized TMGa out and into the reactor chamber.

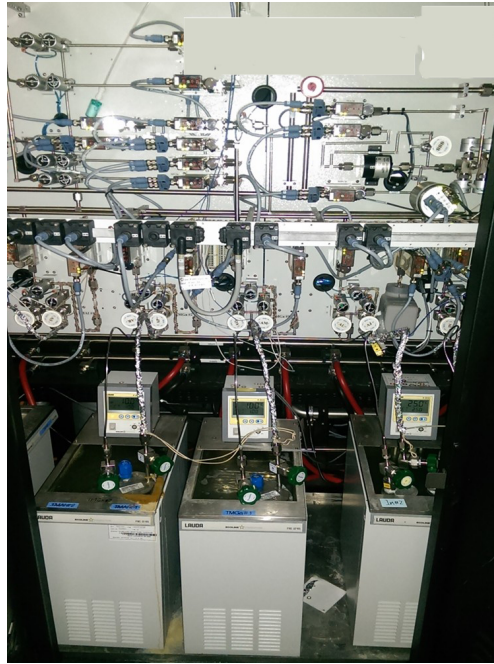


Figure 6.7: CVD Gas Panel and Bubbler. Source: Google Image Search

6.2.7 Measurement System

Measurement system consist of various pressure sensors, thermocouples, and non-intrusive measuring devices. Pressure transducer are place in many areas to monitor and regulate pressure throughout the different systems and in particular, the reactor chamber. During growth, gases are being flow into the chamber and the pressure transducer make sure that the internal pressure does not exceed the users limit. Thermocouples are also place in various areas to monitor temperature throughout the system. However, the susceptor surface has a non-intrusive way to measure temperature. This device is called Pyrometer. Surface temperature is measured using sensor that detect thermal radiations. At higher temperature, thermocouples have prone to have errors duce to conduction and radiation. Pyrometer can be emissivity corrected and can accurately measure true surface temperature. Another non-intrusive metering device measures film thickness. Using the photo reflectance technique, In-situ or real time measurement of film thickness can be acquire. Placing multiple reflectance meters in different area provides thickness monitoring across the susceptor.

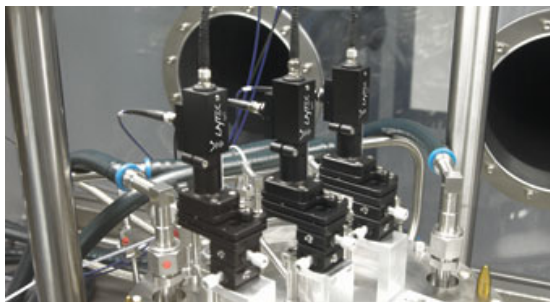


Figure 6.8: In situ Pyrometer and Reflectance Meter.

6.2.8 Computer Electronic System

As described in the previous sections, there are systems that controls the flow rate and concentrations into the reactor chamber, there are pressure sensor to make sure the pressure are within the user limits, temperature sensors to measure system and surface temperatures, and a real time thickness measurement to make sure there are film growth and uniformity. All of the system are link to the main computer electronic system and software, where it controls, monitors, and records data. The software ties all the systems together and simplified user controls. Software can be setup to be automated once the reactor chamber closes. Certain sequential task can be setup to run the CVD system. This sequential task is called a "recipe" in the industry. It is list of commands to open and close valves, increase or decrease power to the heaters, turn mass flow controllers on and off for gas delivery. On some high volume system, robotics can be incorporated and controls handling of susceptor, where it moves finish product onto a rack, and loads in more empty substrates for the next batch of crystal growth. In Fig. 6.9, shows an example of how the software controls all the subsystems. There are feedbacks where user can monitors all conditions and make sure everything is running the way it is.

6.3 Computational Setup

The practical CVD reactor that is being use for this section of the modeling has a different geometry compared to the simple model geometry that was previously used. The

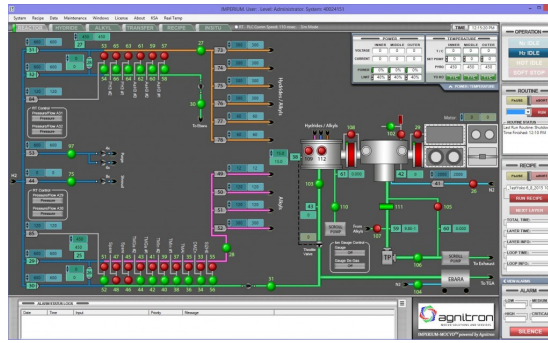


Figure 6.9: Computer Electronic System Control Screen.

overall height has been reduced. This geometry modification reduce the effect of recirculation between the flow path and the exit as seen in the previous cases. Large inlet diameter is also part of the design modifications to help with overall flow uniformity in the system. This model is very similar to the practical CVD reactor, however it is not identical. Due to the company's agreement, the current model will not have its dimension shown. Fig. 6.10 shows the reactor's control volume. Beside the overall dimension change, the boundary conditions remains the same. The inlet, outlet, susceptor, and the flow guide. Keeping simplicity will reduces computational errors. The 11 equations model will be used to model the experimental samples to reduce computation time.



Figure 6.10: Model Geometry for the Practical CVD Reactor

6.4 Computational Results Using Experimental Conditions

There are six samples that will be analyze. Each samples has specific conditions and they will be listed. Similar to the previous chapters, temperature gradient, flow streamlines and deposition will be looked at. Finally, a comparison with the experimental

sample will be discuss. Average time for the process are between 60 minutes to 120 minutes. The results from the computational model will be growth over the entire susceptor. All the conditions has been tuned for this reactor geometry, therefore it is assume that flow streamlines and temperature gradient wont be chaotic as the model in the previous chapter. Computational results will be compared with experimental results such as film thickness and profile map. Advance microscopy can use as well to determine corresponding material structure of the sample. X Ray Diffraction graph can give a insight to how well the crystal is being grown. An Atomic Force Microscopy image can determine the local height and profile of the sample.

6.4.1 Sample PR05

PR05 has a flow concentration of 41.56% Nitrogen, 29.01% Hydrogen, 29.01% Ammonia, and 0.42% TMGa. Reactor pressure to set at 200 Torr, the susceptor rotational speed at 450 RPM, susceptor heater temperature at 1020 C or 1293 K. The mass flow rate is set to be 5.563×10^{-3} kg/s which convert to 3.68 m/s. Summary of all the condition is show in the Fig. 6.11 below.

GaN Condition - PR05			
Pressure (Torr)	200	Nitrogen	41.56%
Rotation (RPM)	450	Hydrogen	29.01%
Heater Temp (C)	1020	Ammonia	29.01%
Inlet mass flow (kg/s)	0.005563	TMGa	0.42%

Figure 6.11: Reactor Condition for GaN Growth - Sample PR05

Temperature contours for PR05 was very uniform, the thermal boundary layers are very thin and close to the susceptors and it does not have any thermal recirculation. Buoyancy effect is keep in control by the susceptor rotation and the main bulk flow. Fig. 6.12 shows the temperature contour profile.

Fig. 6.13 shows the velocity streamlines for sample PR05. The flow streamlines are very laminar, flow from the center bends and flow toward the exit. Rotation speed is not over dominating causing swirls in the system. Average flow velocity is about 4 m/s and as it exit the velocity increases to around 6 m/s due to the reducing exit area.

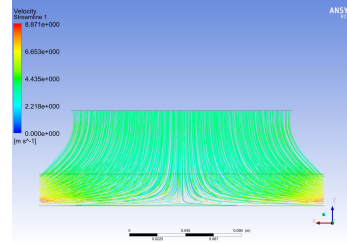
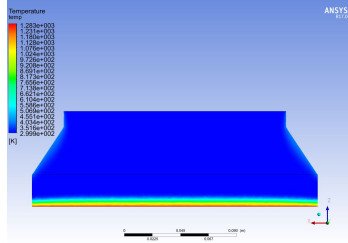


Figure 6.12: Temperature Contour - Figure 6.13: Velocity Streamlines -
Sample PR05

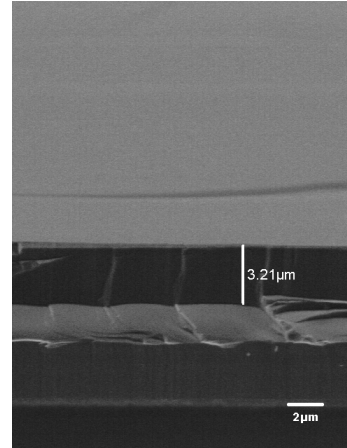
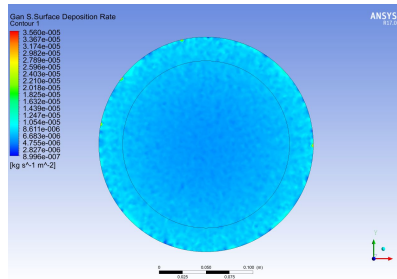


Figure 6.14: GaN Deposition Contour - Sample PR05
Figure 6.15: SEM Image - Sample PR05

In Fig. 6.14 shows the GaN deposition rate across the susceptor. The entire susceptor region is covered in blue indicating a very uniform deposition across the susceptor. The edges are darker due to edge effects and can be ignored. Average deposition rate is found to be around 6.12×10^{-6} kg/s-m² which converts to 3.58 microns per hour. This growth rate is inside the range of what was predicted by the industry. Using the ISI SEM at Rutgers MERL, thickness data was measured and recorded. Fig. 6.15 shows the measured thickness at the center of the wafer to be 3.21 microns. The percent difference for this sample conditions is about 11.5%.

A SEM image can show much more information than just the thickness. It can show the microstructure of the film. The microstructure of the film depends on the growth conditions. If the concentration ratio is high, and growth temperature is also high, micro hexagonal defects would form. Knowing the reason why these defects occur can help the user narrow down a specific operation conditions to improve film quality.

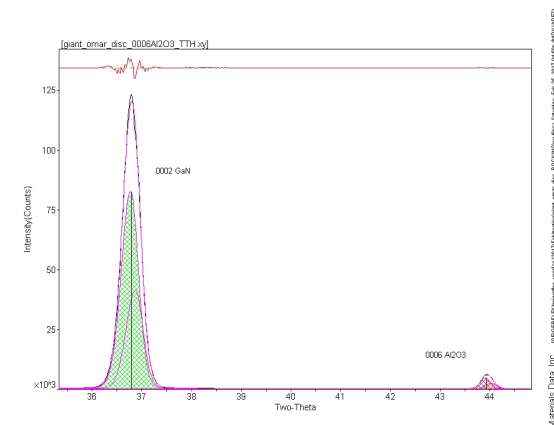


Figure 6.16: X Ray Diffraction Graph - Sample PR05

In addition to the SEM image, a XRD for this sample has also been taken. The XRD graph is shown on the Fig. 6.16. XRD rocking curve tells how well the crystal lattice is arranged. If the crystal lattice has no defects and no strain, the intensity is long and narrow and along the diffraction line. If the lattice experiences uniform strain, the peak would also be tall and narrow but the amplitude is off centered. If the lattice is non uniform, then the curve has a lower intensity and is wider. In Fig. 6.16, the tall and narrow curve resembles the GaN crystal lattice. The curve is a bit off centered to the right indicating that the structure experiences some form of uniform strain. However, this sample still has overall excellent crystallinity.

6.4.2 Sample PR06

PR06 has a flow concentration of 41.56% Nitrogen, 29.01% Hydrogen, 29.01% Ammonia, and 0.42% TMGa. Reactor pressure is set at 200 Torr, the susceptor rotational speed at 450 RPM, susceptor heater temperature at 1040C or 1313K. The mass flow rate is set to be 5.563×10^{-3} kg/s which converts to 3.68 m/s. Summary of all the conditions is shown in the Fig. 6.17 below. The main difference for this sample was susceptor temperature was increased to 1313K.

In Fig. 6.18 shows the temperature contour for sample PR06. Even with the higher temperature, the temperature contour is still very uniform across the susceptor. The

GaN Condition - PR06			
Pressure (Torr)	200	Nitrogen	41.56%
Rotation (RPM)	450	Hydrogen	29.01%
Heater Temp (C)	1040	Ammonia	29.01%
Inlet mass flow (kg/s)	0.0055626	TMGa	0.42%

Figure 6.17: Reactor Condition for GaN Growth - Sample PR06

thermal boundary layer remain thin and coherent to the surface.

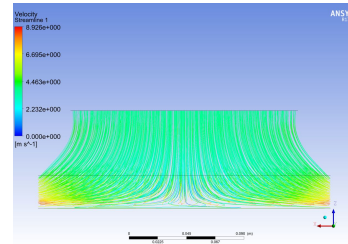
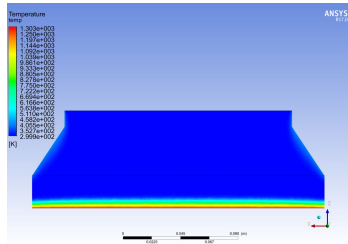


Figure 6.18: Temperature Contour - Figure 6.19: Velocity Streamlines - Sample PR06

Fig. 6.19 shows the velocity streamlines for sample PR06 and it is very similar to Fig. 6.13. Mass flow rate was not change, and the rotational speed was not change, therefore, the overall flow characteristic should not be affected. The forces from the buoyancy is keep under control by the bulk flow and the rotation.

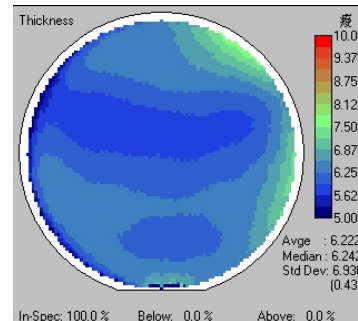
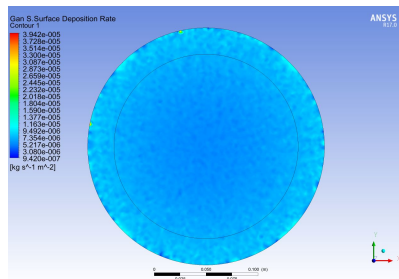


Figure 6.20: GaN Deposition Contour - Sample PR06
Figure 6.21: Thickness Layer Contour - Sample PR06

The overall uniformity of the susceptor also remain very well. As seen in Fig. 6.20, the entire susceptor is cover in the blue color indicating constant uniformity across, ignoring the edge effect. Because of the increase in temperature, the deposition rate also seems to be increase. With an average deposition rate of 5.88×10^{-6} kg/s-m² or

3.44 microns per hour. This makes sense, since the concentration was not change, the deposition rate should not change or if it does it should not change that much. For this condition, an experimental thickness layer map was acquired by the use of a Nanometrics Film Thickness measurement machine. Fig. 6.21 was measured with the average thickness to be 6.222 microns. Multiplying the total process time by the deposition rate gives 6.88 microns. Percent difference is calculated to be 10.6%. SEM image was also taken for this sample. Using the Rutgers MERL's SEM system, the image is shown in Fig. 6.22. The measure thickness at the center of the wafer is 7.9 microns.

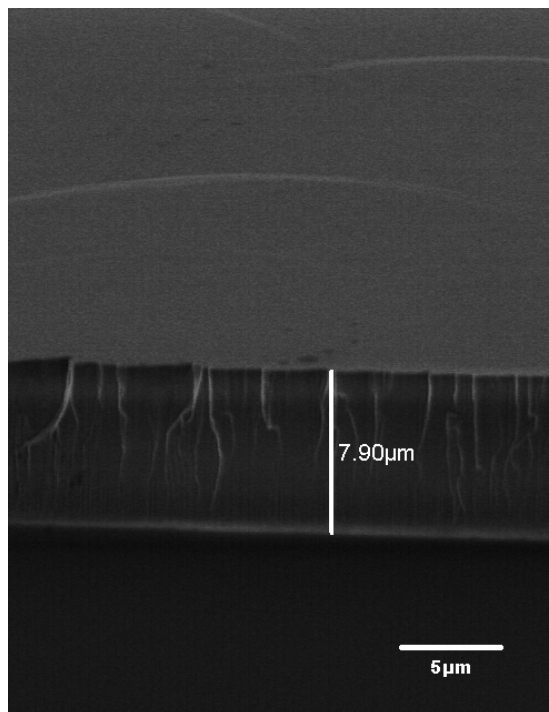


Figure 6.22: SEM Image - Sample PR06

6.4.3 Sample PR07

PR07 has a flow concentration of 41.49% Nitrogen, 29.05% Hydrogen, 29.05% Ammonia, and 0.41% TMGa. Reactor pressure to set at 200 Torr, the susceptor rotational speed at 300 RPM, susceptor heater temperature at 1040C or 1313K. The mass flow

rate is set to be 5.568×10^{-3} kg/s which convert to 3.69 m/s. Summary of all the condition is show in the Fig. 6.23 below. For this sample, the concentration of Hydrogen and Ammonia has increased both by 0.04% and Nitrogen was decreased by 0.07% and TMGa decreased by 0.01%. This causes the flow to be a quicker by 0.01 m/s. Rotation speed has been also been decreased by 150 RPM.

GaN Condition - PR07			
Pressure (Torr)	200	Nitrogen	41.49%
Rotation (RPM)	300	Hydrogen	29.05%
Heater Temp (C)	1040	Ammonia	29.05%
Inlet mass flow (kg/s)	0.005568	TMGa	0.41%

Figure 6.23: Reactor Condition for GaN Growth - Sample PR07

Even though there are many changes in the conditions, the overall temperature profile remains very similar. Fig. 6.24 shows no changes to the contour levels and the thermal thickness.

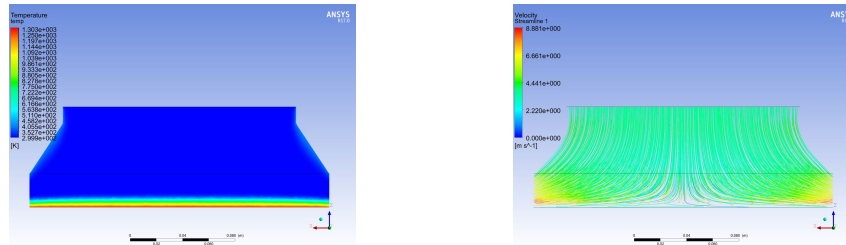


Figure 6.24: Temperature Contour - Figure 6.25: Velocity Streamlines - Sample PR07

In the velocity streamline shown in Fig. 6.25, it also shows no changes. The only changes is the max limit has been decreased from 8.926 m/s in Fig. 6.19 to 8.881 m/s in the current figure. Looking at Fig. 6.26, the overall uniformity continue to be excellent indicated by the single shade of blue across the susceptor. However, the deposition rate seems to have decrease to an average of 5.48×10^{-6} kg/s-m² or 3.21 micron per hour. This is due to the decrease in the TMGa concentration in the bulk flow. The thickness contour map is shown in Fig. 6.27. The average thickness is measured to be 6.147 microns. Using the total process time, the computational thickness is calculated to be 6.42 microns. The percent difference in this condition is about 4.4%.

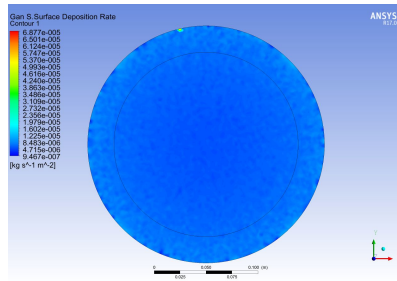


Figure 6.26: GaN Deposition Contour - Sample PR07

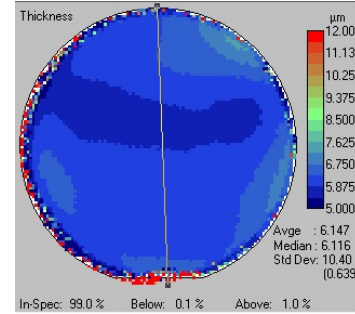


Figure 6.27: Thickness Layer Contour - Sample PR07

6.4.4 Sample PR08

PR08 has a flow concentration of 41.53% Nitrogen, 29.07% Hydrogen, 29.07% Ammonia, and 0.33% TMGa. Reactor pressure to set at 200 Torr, the susceptor rotational speed at 300 RPM, susceptor heater temperature at 1040C or 1313K. The mass flow rate is set to be 5.563×10^{-3} kg/s which convert to 3.06 m/s. Summary of all the condition is show in the Fig. 6.28 below. For this case, Nitrogen was increased by 0.04%. Hydrogen and Ammonia is both are increased by 0.02% and further decreased TMGa concentration by 0.08%. Decreasing TMGa caused the overall flow velocity to drop 0.62 m/s.

GaN Condition - PR08		
Pressure (Torr)	200	Nitrogen 41.53%
Rotation (RPM)	300	Hydrogen 29.07%
Heater Temp (C)	1040	Ammonia 29.07%
Inlet mass flow (kg/s)	0.00460926	TMGa 0.33%

Figure 6.28: Reactor Condition for GaN Growth - Sample PR08

Fig. 6.29 shows no changes and thermal boundary layer remains uniform. For the velocity streamlines, the overall maximum flow speed was decreased to 7.435 m/s from 8.881 m/s from Fig. 6.25. Otherwise, the overall flow streams are very uniform and laminar.

Due to the decrease in the TMGa concentration, the number of reaction decreases causing deposition rate to fall. With an average deposition rate of 5.13×10^{-6} kg/s-m² or

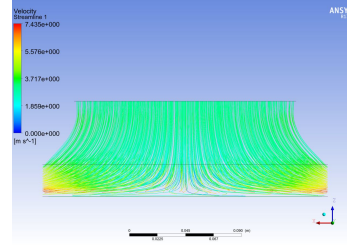
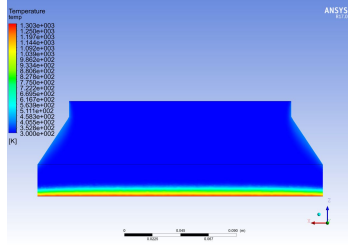


Figure 6.29: Temperature Contour - Figure 6.30: Velocity Streamlines -
Sample PR08 Sample PR08

3.00 microns per hour. Even though the deposition rate is low compare to the previous condition, it is predicted to be lower since the TMGa concentration decreases. Looking at the experimental thickness contour in Fig. 6.32, the average thickness is measured to be 6.399. Take the deposition rate and the total process time, the computational thickness is calculated to be 6 microns. The percent difference for this condition is around 6.2%. PR09 was an identical sample with PR08, therefore PR09 will not include in the study.

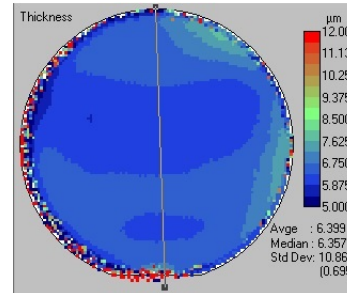
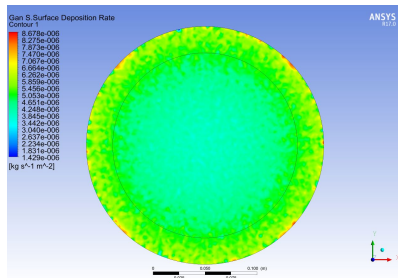


Figure 6.31: GaN Deposition Contour Figure 6.32: Thickness Layer Contour
- Sample PR08 - Sample PR08

6.4.5 Sample PR10

PR10 has a flow concentration of 25.64% Nitrogen, 34.48% Hydrogen, 39.26% Ammonia, and 0.62% TMGa. Reactor pressure to set at 200 Torr, the susceptor rotational speed at 300 RPM, susceptor heater temperature at 1050 C or 1323 K. The mass flow rate is set to be 8.377×10^{-3} kg/s which convert to 6.42 m/s. Summary of all the condition is show in the Fig. 6.33 below. In this sample, there are big changes to the flow concentration. Nitrogen concentration has been reduced by nearly half, and a

big increase in the Hydrogen and Ammonia concentration. Susceptor heater was also increase. The outcome of these changes are shown below.

GaN Condition - PR10			
Pressure (Torr)	200	Nitrogen	25.64%
Rotation (RPM)	300	Hydrogen	34.48%
Heater Temp (C)	1040	Ammonia	39.26%
Inlet mass flow (kg/s)	0.00837729	TMGa	0.62%

Figure 6.33: Reactor Condition for GaN Growth - Sample PR10

The temperature contour are similar to previous cases as seen in Fig. 6.34. Flow streamlines remains laminar and no recirculation flow are seen in this condition as well. Overall velocity has been increased with flow averaging around 7 m/s. Maximum limit on Fig. 6.35, shows 14.67 m/s which is much higher than the previous case.

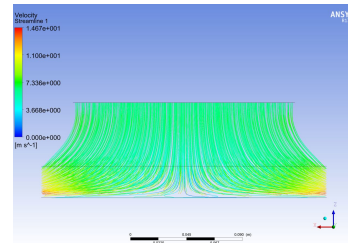
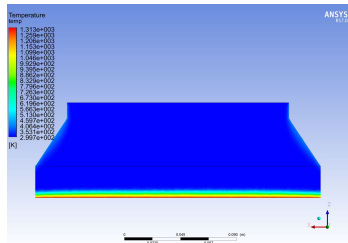


Figure 6.34: Temperature Contour - Figure 6.35: Velocity Streamlines - Sample PR10

With all the previous case having deposition rate between 3-4 microns per hour, this condition changes the deposition rate the most. In Fig. 6.36, shows the contour map for the GaN deposition rate. The average deposition rate was calculated to be 8.58×10^{-6} kg/s-m² or 5.02 microns per hour. Film thickness contour map was also presented in this case, and shown in Fig. 6.37. The average thickness measured was 5.272 microns. The computational thickness is calculated to be 5.02 microns taking growth time to be 1 hour. The percent difference between the two data is around 4.8%.

In this sample, an AFM image was performed and shown in Fig. 6.38. It is a 20 micron resolution using a tapping mode measuring probe. The result shows the local height of surface. In this image, the scale maximum shown in white is 167.8 picometer and lowest scale shown in black is -178.1 picometer. Analyzing the image shows the

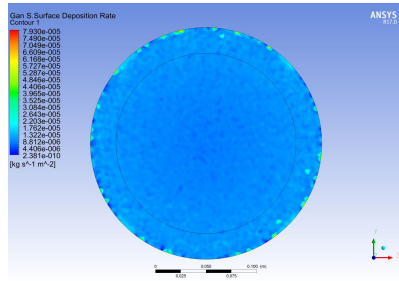


Figure 6.36: GaN Deposition Contour - Sample PR10

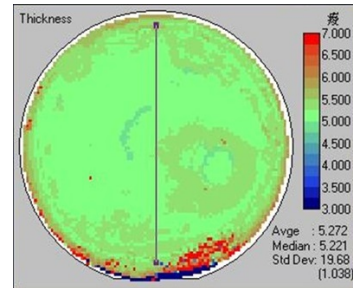


Figure 6.37: Thickness Layer Contour - Sample PR10

overall color is brown indicating the change in height is very small. There are some island formation on the surface as seen in the white spots, however, the change is in the scale of picometer. Overall the surface morphology of this sample is very well grown. Surface morphology is very important to GaN growth, if the image shows excessive islands or steps, that indicates temperature might not be optimized or concentration ratio might be too high. Further adjustment can be made to the operating conditions to improve film quality.

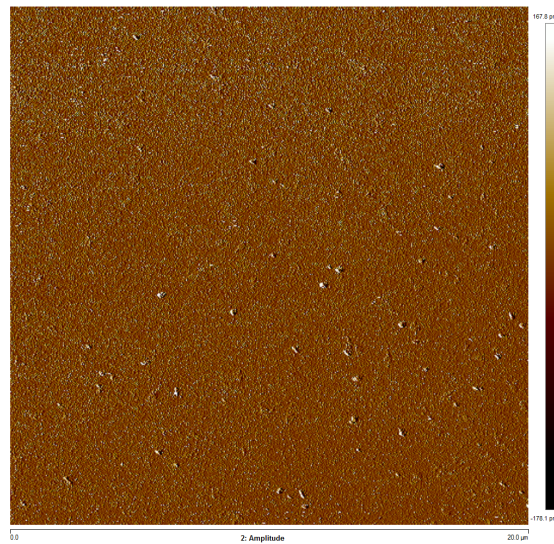


Figure 6.38: Atomic Force Microscopy Image - Sample PR10

6.4.6 Sample PR11

PR11 has a flow concentration of 0% Nitrogen, 70.60% Hydrogen, 29.07% Ammonia, and 0.33% TMGa. Reactor pressure to set at 200 Torr, the susceptor rotational speed at 300 RPM, susceptor heater temperature at 1040C or 1313K. The mass flow rate is set to be 4.125×10^{-3} kg/s which convert to 5.71 m/s. Summary of all the condition is show in the Fig. 6.39 below. For this sample, the Nitrogen is taken out of the bulk gas concentration and carrier gas is solely Hydrogen. As seen in the previous chapter, Hydrogen is a very light gas and the effect of buoyancy increases when more of Hydrogen is used. The effect is more dominating in the center and less dominating near the edge.

GaN Condition - PR11		
Pressure (Torr)	200 Nitrogen	0.00%
Rotation (RPM)	300 Hydrogen	70.60%
Heater Temp (C)	1040 Ammonia	29.07%
Inlet mass flow (kg/s)	0.004125 TMGa	0.33%

Figure 6.39: Reactor Condition for GaN Growth - Sample PR11

Observing the results for the temperature contour and the velocity streamlines seems similar to the previous cases. Thermal boundary layers are still very uniform and coherent. Average flow speed is around 6.5 m/s. Fig. and Fig. are the temperature contour and streamlines respectively. The biggest changes occurs in the deposition rates as predicted. In Fig. 6.42, you can clearly see the difference in the deposition rate at the center and at the outer part of the susceptor. At the center, it is to be around 1.17 microns per hour, while the outer portion is around 1.75 microns per hours. Even though the numbers does not seem to be that far apart, it can affect the quality of the film. The average deposition rate across the susceptor is found to be 2.41×10^{-6} kg/s-m² or 1.41 microns per hour.

6.5 Conclusion

In this chapter, an in-depth analysis was done on the GaN samples provided by the industry. Using the 11 equation model, a very similar geometry model was created to

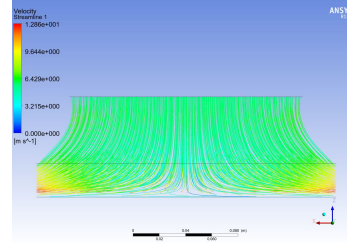
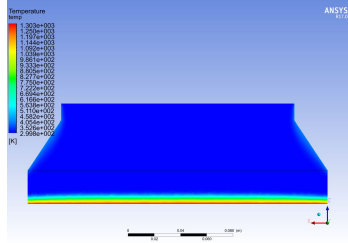


Figure 6.40: Temperature Contour - Figure 6.41: Velocity Streamlines -
Sample PR11

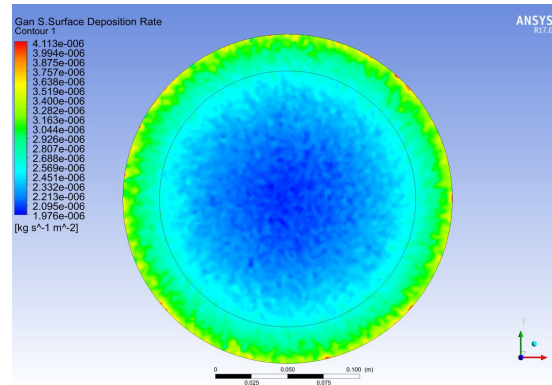


Figure 6.42: GaN Deposition Contour - Sample PR11

model the actual practical CVD reactor. Using the 11 chemical pathway model, all six sample were simulated computationally. Each of the six samples has different parameters. Since the parameter are already optimized for the geometry, flow streamlines and the heat transfer were almost ideal. Laminar streamlines goes from inlet to outlet. Rotational speed is just enough to overpower the buoyancy effect. Thermal gradient boundary layers were very uniform and thin. There are no waves and no recirculation of any type. However, with each different parameter, the deposition rate were different even though the flow and thermal results are all almost similar. The computational results was compared with the experimental data such as film thickness map by using a profilometer and SEM image by using the SEM at Rutgers MERL. Additional advance microscopy can be used to examine the microstructure and surface morphology of the material. Knowing the cause of structural defects can improve film quality. In the future work, a Transmission Electron Microscopy or TEM image would give even

greater information such as internal structure, crystal arrangement, and defects.

Chapter 7

Conclusions

7.1 Summary

In this thesis, computational model was setup to study and investigate the Gallium Nitride Chemical Vapor Deposition Reactor. An in-depth study of flow characteristics and heat transfer of the system will be discuss in this thesis. CVD is a heat activated process that allow material to break down atomically and recombine to form layers of crystalline structures. Maintaining the proper flow rate of the gases, temperature of the heater and the pressure of the system is very important to the quality of the film growth. Therefore, it is important to understand the importance of these operating parameters and how it affect the outcome. There are going to be four steps in this study. The first step is to create a simple geometry model that has Air, heat transfer and fluid flow. Second is to modify the simple geometry model to incorporate different type of species. Instead of Air, Hydrogen and Nitrogen will be used. Third is to incorporate a chemistry model into the simple geometry design. The final step is to apply the same chemical computational model to a reactor geometry model and collect and analyze data.

Step one of the modeling was to create a simple geometry design. The design was adapted from the experimental model that was used in the master thesis. It was a simple cone shape design used for the flow guide. Taking the volume between the flow guide and the susceptor, the simple model was created. The idea was to use this geometry model to be the basis of all the computational model. With just temperatures, flow velocities and streamlines data, one can determine the flow characteristic and heat transfer in the reactor. The results can show if the flow is laminar or turbulent, as well as if buoyancy force dominate or forced convection dominates inside the reactor.

Step two models the reactor with chemical species. Since most industry uses carrier

gases to transport the precursor gas and reactant gas into the chamber. Modeling the carrier gases was a way to predict how the flow behaves when it entered a low pressure, high temperature chamber. The results shows that Hydrogen is a gas with very small mass. Effect of buoyancy is greater for lighter molecules. However hydrogen is needed to aid deposition, therefore it cannot be taken out. So this study in different concentration of Nitrogen and Hydrogen was needed to find the optimal combination.

Step three was to implement the full chemistry model. The original chemistry model was adapted from Sengupta et al. It has a total of 17 gas reactions and 52 surface reactions totaling 69 chemical pathways. Solving the computational model for the 69 chemical pathways was very difficult. Some of the pathway were very stiff, and requires a more stable solver. The more stabilized the solver the longer it will take to solve. When Hu et al, was able to reduce the model down to 11 chemical pathways. It was a preferred action to take the 11 pathway for the computational model. However, because it's simpler model, many conditions were limited to specific ranges. One condition was the susceptor temperatures cannot be under 1000K. In later comparison, the 11 chemical pathway were closer to experimental results.

The final step was to take the refined 11 chemical pathway model and applied it to a practical CVD reactor. Using real conditions and geometry that is close to the real CVD reactor system, similar gallium nitride growth results was able to obtain. Validating computational results with experimental results will help reduce the cost when optimizing the operating conditions since the only resource waste is computing time rather than the high expensive raw materials. In addition, using advanced microscopy such as XRD and AFM, can increase the insight to what operating conditions causes structural defects. Improving growth conditions will no longer be trial and error, but rather by use of computational models to optimize the results. Many of the CVD industries and university starting to invest funds into computational study instead of experimental study. The reason is computational study require lesser cost to operate. Also computational study give a better insight to the problem once the model has been verified and validated. To further advance the technology, optimization will be needed.

7.2 Future Work

- More comparison of experiment sample with micro-structural and material data from advance microscopy.
- Continue to improve the solution to the simplified 11 chemical pathway model. Further valid results with more experimental data
- Optimization of the computational model to yield an optimal operating parameters and condition to applied to a commercial reactors
- Reactor Design - changing geometry to improve flow and growth conditions
- Introduce transient study

Bibliography

- [1] H. P. Maruska, W. C. Rhines, A Modern Perspective on the History of Semiconductor Nitride Blue Light Sources. *Solid-State Electronics*, 2015.
- [2] M.Ritala, J. Niinisto, S. Krumdieck, P. Chalker, H Aspinall, M. Pemble, W. Gladfelter, B.Leese, R.Fischer, H. Parala, R. Kanjolia, R. Dupuis, S. Alexandrov, S. Irvine, R. Palgrave, I. Parkin, *Chemical Vapour Deposition*. The Royal Society of Chemistry, 2009.
- [3] M. Konuma, *Thin Film Processes II*. Springer-Verlag, New York, 1992.
- [4] S. Nakamura, M.Krames, History of GalliumNitride-Based Light-Emitting Diodes for Illumination. *Proceedings of the IEEE*, 2013.
- [5] R. Juza. H. Hahn, Uber Die Kristallstrukturen von Cun, GaN und Inn Metallamide und Metallnitride. *Zeitschrift Fur Anorganische und Allgemeine Chemie*, 1938.
- [6] H. P. Maruska, J. J. Tietjen, The Preparation and Properties of VaporDeposited SingleCrystalLine GaN. *Applied Physics Letter*, 1969.
- [7] S. Yoshida, S. Misawa, S. Gonda, Improvements on the Electrical and Luminescent Properties of Reactive Molecular Beam Epitaxially Grown GaN Films by Using AlNCoated Sapphire Substrates. *Applied Physics Letter*, 1983.
- [8] T. Kawabata, T. Matsuda, S. Koike, GaN Blue Light Emitting Diodes Prepared by Metalorganic Chemical Vapor Deposition. *Journal of Applied Physics*, 1984.
- [9] H. Amano, N. Sawaki, I. Akasaki, Y. Toyoda, Metalorganic Vapor Phase Epitaxial Growth of a High Quality GaN Film Using an AlN Buffer Layer. *Applied Physics Letters*, 1986.

- [10] S. Nakamura, T. Mukai, M. Senoh, Candela Class High Brightness InGaN/AlGaN Double Heterostructure Blue Light Emitting Diodes. *Applied Physics Letter*, 1994.
- [11] C. Nickolas, *Introduction to GaN Technology*, <http://www.digikey.com>, 2011.
- [12] T. Palacios, K. Mishra, S. Kumer, GaN-Based Transistors for High-Frequency Applications. *Reference Module in Materials Science and Materials Engineering*, 2016.
- [13] C. S. Whelan, N. J. Koliass, S. Brierley, C. MacDonald, S. Bernstein, GaN Technology for Radars. *CS MANTECH Conference*, Boston, MA, 2012.
- [14] Y. Zhu, Y. Han, Comparison of GaN FET and Si MOSFET Based Vienna Rectifiers. *Energy Conversion Congress and Exposition*, Milwaukee, WI, 2016.
- [15] T. Nishimiya, H. Ogiya, M. Hiramoto S. Motoyama P. Wood, Recess Etching Process for AlGaIn/GaN-HFET Devices Using In-Situ Monitoring. *CS MANTECH Conference*, Denver, CO, 2014.
- [16] E. Belyaev, V.N Bessolov, N.S. Boltovets, S.A Volodymyr, *Physical and Technological Problems of GaN Electronics*. Naukova Dumka, 2016.
- [17] J.A Freitas, N.A Mahadik, T. Sochacki, M. Iwinska, M. Bockowski, J.C Culbertson, HVPE GaN Wafers with Improved Crystalline and Electrical Properties. *Journal of Crystal Growth*, 2016.
- [18] S. Ravasio, Takeshi Momose, Katsushi Fujii, Yukihiro Shimogaki, Masakazu Sugiyama, C. Cavallotti Analysis of the Gas Phase Kinetics Active During GaN Deposition from NH₃ and Ga(CH₃)₃. *Journal of Physical Chemistry*, 2015.
- [19] J. R. Creighton, P. Ho, Introduction to Chemical Vapor Deposition. *Chemical Vapor Deposition*, 2001.
- [20] D. Sengupta, S. Mazumder, W. Kuykendall, S. Lowry, Combined Ab Initio Quantum Chemistry and Computational Fluid Dynamics Calculations for Prediction of Gallium Nitride Growth. *Journal of Crystal Growth*, 2005.

- [21] A. Hirako, K. Kusakabe, K. Ohkawa, Modeling of Reaction Pathways of GaN Growth by Metalorganic Vapor-Phase Epitaxy using TMGa/NH₃/H₂ system: A Computational Fluid Dynamics Simulation Study. *Japanese Journal of Applied Physics*, 2005.
- [22] Hu, C.; Chen, C.; Wei, T.; Li, T. T.; Wang, C. C.; Huang, C. Y.; Lin, Y, A Simplified and Universal Mechanism Model for Prediction of Gallium Nitride Thin Film Growth Through Numerical Analysis *International Journal of New Technology and Research*, 2016.
- [23] S. Wong, Y. Jaluria, Numerical Simulation of a Practical Chemical Vapor Deposition Reactor. *Numerical Heat Transfer*, 2016.
- [24] J. Meng, S. Wong, Y. Jaluria, Fabrication of GaN Films in a Chemical Vapor Deposition Reactor. *ASME Journal of Thermal Systems*, 2015.
- [25] Franklyn J. Kelecyc. Coupling Momentum and Continuity Increases CFD Robustness, *ANSYS*, 2008.
- [26] Jiandong Meng, Yogesh Jaluria, Transient Behavior of Thin-Film Deposition: Coupling Micro- and Macro-Scale Transport. *Numerical Heat Transfer*, 2015.
- [27] Jiandong Meng, *SIMULATION AND OPTIMIZATION OF THE GAN MOCVD PROCESS*. Ph.D thesis, Rutgers University, 2014.
- [28] Jiandong Meng, Yogesh Jaluria, Thermal Transport in the Gallium Nitride Chemical Vapor Deposition Process. In *ASME 2013 Heat Transfer Summer Conference*, Minneapolis, MN, 2013.
- [29] Jiandong Meng, Yogesh Jaluria, Numerical Simulation of the GaN Growth Process in a MOCVD process. *The Electrochemical Society*, 2011.
- [30] S. J. Pearton, R. J. Shul, R. G. Wilson, F. Ren, J. M. Zavada, C. R. Abernathy, C. B. Vartuli, J. W. Lee, J. R. Mileham, J. D. Mackenzie, The Incorporation of Hydrogen into III-V Nitrides During Processing. *Journal of Electronic Materials*, 1996.

- [31] C.K. Hu, C.J. Chen, T.C. Wei, T. Li, C. Y. Huang, C.L. Chao, Y.J. Lin, Numerical Verification of Gallium Nitride Thin Film Growth in a Large MOCVD Reactor. *Coatings*, 2017.
- [32] V. Harutyunyan, A. Aivazyan, E. Weber, Y. Kim, Y. Park, S. G. Subramanya, High Resolution X-Ray Diffraction Strain-Stress Analysis of GaN/Sapphire Heterostructures. *Journal of Physics: Applied Physics*, 2000.
- [33] J. G. Eden. *Film Deposition by Plasma Techniques*. J. L. Vossen and W. Kern, Academic Press, New York, 1991.
- [34] H.O. Pierson. *Handbook of Chemical Vapor Deposition (CVD): Principles, Technology, and Applications*. CVD : PRINCIPLES, TECHNOLOGY, AND APPLICATIONS. Noyes Publications, 1992.
- [35] Chiu, Wilson, Richards-Cristy, Jaluria Yogesh, Experimental and Numerical Study of Conjugate Heat Transfer in a Horizontal Channel Heated from Below. *Journal of Heat Transfer*, 688–697, 2001.
- [36] Bei Wu, Ronghui Ma, Hui Zhang, Epitaxy Growth Kinetics of GaN Films. *Journal of Crystal Growth*, 2003.
- [37] K. Mazaev, A. Lobanova, E. Yakovlev, R. Talalaev, A. Galyukov, Y. Makarov, D. Gotthold, B. Albert, L. Kadinski, and B. Peres, Modeling and Experimental Analysis of AlGa_N MOVPE in Commercial Vertical High-Speed Rotating-Disk Reactors. *Journal of Crystal Growth*, 190–196, 2004.
- [38] L. Kadinski, V. Merai, A. Parekh, J. Ramer, E.A. Armour, R. Stall, A. Gurary, A. Galyukov, Y. Makarov Computational Analysis of GaN/InGa_N Deposition in MOCVD Vertical Rotating Disk Reactors. *Journal of Crystal Growth*, 2004.
- [39] Fujio Terai, Hiroaki Kobayashi, Shuji Katsui, Naoki Tamaoki, Takao Nagatomo, and Tetsuya Homma. High-Speed Rotating-Disk Chemical Vapor Deposition Process for In-Situ Arsenic-Doped Polycrystalline Silicon Films. *Japanese Journal of Applied Physics*, 7883, 2005.

- [40] Ran Zuo, Hong Zhang, Xiang Lin Liu, Transport Phenomena in Radial Flow MOCVD Reactor with Three Concentric Vertical Inlets. *Journal of Crystal Growth*, 2006.
- [41] Yuh-Renn Wu, Jasprit Singh, Transient Study of Self-Heating Effects in Al-GaN/GaN HFETs: Consequence of Carrier Velocities, Temperature, and Device Performance. *Journal of Applied Physics*, 2007.
- [42] Kwong Yam Fong, Li Low Li, Ann Oh Sue, Zainuriah Hassan Gallium Nitride: An Overview of Structural Defects. *Intech Open*, 2011.
- [43] A. Zhou, Xiang Qian Xiu, Rong Zhang, ZiLi Xie, Xue Mei Hua, Bin Liu, Ping Han, Shu Lin Gu, Yi Shi, You Dou Zheng, Roles of V/III Ratio and Mixture Degree in GaN Growth: CFD and MD Simulation Study. *Chinese Physical Society*, 2013.
- [44] H.S Fang, Y. Y. Pan, J.A Wei, S. Liu, Z. Zhang, L.L. Zheng, Numerical Study and Optimization of GaN Thin Film Growth by MOCVD Method. *ASME Heat Transfer Summer Conference 2013*, Minneapolis, MN, 2013.
- [45] W. Wang, W. Yang, Z. Liu, Y. Lin, S. Zhou, H. Qian, F. Gao, G. Li, Epitaxial Growth of High Quality AlN Films on Metallic Aluminum Substrates. *CrystEngComm*, 4100–4107, 2014.
- [46] Wonkyun Yang Junghoon Joo, Numerical Modeling for GaN deposition by MOCVD: Effect of the Gas Inlet. *Applied Science and Convergence Technology*, 2014.
- [47] E Raj, Z Lisik, P Niedzielski, L Ruta, M Turczynski, X Wang, A Waag Modeling of MOCVD Reactor: New 3D Approach. *Journal of Physics: Conference Series*, 2014.
- [48] Chien-Fu Tseng, Tsung-Yen Tsai, Yen-Hsiu Huang, Ming-Tsang Lee, Ray-Hua Horng Transport Phenomena and the Effects of Reactor Geometry for Epitaxial GaN Growth in a Vertical MOCVD Reactor. *Journal of Crystal Growth*, 2015.

- [49] David S. Dandy, Jungheum Yun, Momentum and Thermal Boundary-Layer Thickness in a Stagnation Flow Chemical Vapor Deposition Reactor. *Journal of Materials Research*, 12:1112–1121, 1997.
- [50] Sun, J., Redwing, J., Kuech, T., Model Development of GaN MOVPE Growth Chemistry for Reactor Design *Journal of Electronic Materials*, 2000.
- [51] Timoshkin, A. Y., Bettinger, H. F., Henry F. Schaefer, III, DFT Modeling of Chemical Vapor Deposition of GaN from Organogallium Precursors. Thermodynamics of Elimination Reactions *Journal of Physical Chemistry*, 2000.
- [52] Tropea, C., Yarin, A., Foss, J., *Springer Handbook of Experimental Fluid Mechanics*. Springer, New York, NY, 2007